Silicates as an Explanation for Discrepancies in Atmospheric Modeling of L-Type Brown Dwarfs

Zacory Shakespear

Submitted to Brigham Young University in partial fulfillment
of graduation requirements for the degree of
Bachelor of Science

Denise Stephens, Advisor
Benjamin Boizelle, Reader
Karine Chesnel, Honors Coordinator

Department of Physics and Astronomy

Brigham Young University

ABSTRACT

Silicates as an Explanation for Discrepancies in Atmospheric Modeling of L-Type Brown Dwarfs

Zacory Shakespear
Department of Physics and Astronomy, BYU
Bachelor of Science

Forward retrieval modeling is a powerful method for classifying brown dwarf atmospheres and their physical parameters. However, the results of this method are only as good as the models compared against the data. Silicates in the atmospheres of L-type brown dwarfs have been shown to cause model overfitting around $10\mu m$, but it is not known what impact, if any, these silicates have on other portions of brown dwarf atmospheric spectra. I report a preliminary negative correlation between model overfitting at $10\mu m$ and model underfitting from $3.5-4.25\mu m$ using spectra from two L-dwarfs from JWST and seven L-dwarfs combined from NASA's IRTF telescope, the AKARI space telescope, and the Spitzer space telescope. I also report on the impact of combining spectra on forward retrieval modeling results and discuss the need for JWST data to further explore the strength and causes of this correlation.

Keywords: L dwarfs, infrared astronomy, spectroscopy

ACKNOWLEDGMENTS

I would like to express my gratitude to Dr. Stephens for her mentorship throughout my undergraduate career, as well as her guidance in the production of this thesis. I would also like to thank my committee members for their support throughout the writing process.

I would be remiss if I did not thank Savanah Turner and Crystal-Lynn Bartier for their friendship while I've worked alongside them. Thank you for all the help with research, coding, editing, and citation hunting.

Finally, I would like to thank my wife, Paulee, for her tireless support. Your belief in me has been a constant buoy that I will treasure always.

Contents

List of Figures

List of Tables

Chapter 1

Introduction

Brown dwarfs are celestial objects which are larger than planets, but smaller than stars. They were first theorized by Kumar (1962) as the result of star formation processes below $0.05M_{\odot}$ and their existence verified by Oppenheimer et al. (1995) with the discovery of Gl 229B. Brown dwarfs are now known to be objects with masses $< 70M_{Jup}$ and temperatures ranging from $300K < T < 2000K$ (Cushing 2013). They can orbit around a star or float through space on their own (Dupuy & Liu 2017). Though there is no hydrogen fusion in their core, brown dwarfs glow from the heat of their formation and can be detected by both ground-based and space-based telescopes.

These objects are useful tests for our understanding of stellar and exoplanet formation as well as atmospheric dynamics because of how they straddle the line between stars and planets. Brown dwarfs are cool enough for chemical compounds like CH_4, water, and ammonia to form in their atmospheres, as well as for clouds to appear. They also often exhibit convective mixing, a process they have in common with many types of stars. The markers for these processes are present in their spectra, which scientists can analyze to characterize brown dwarfs and their atmospheric properties.

1.1 Spectroscopy

As mentioned above, brown dwarfs emit light due to their internal heat, much in the same way that a heated light bulb filament emits light in a dark room. This light is a mix of different wavelengths described by Plank's function (Equation 1.1).

$$B_\lambda(T,\lambda) = \frac{2hc^2/\lambda^5}{e^{hc/\lambda kT} - 1} \tag{1.1}$$

As the light passes through the cooler and more diffuse atmosphere, it interacts with the atoms and molecules present. These interactions cause specific wavelengths of light to be absorbed by atoms and molecules. For atoms, these wavelengths are discrete while for molecules, these wavelengths cover a range of values. In addition, processes in the atmosphere, such as cloud formation or the movement of convective cells of gas, can result in the light (or flux) being enhanced or decreased in certain regions.

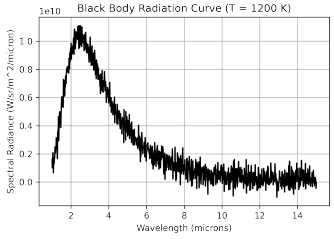

((a)) Model black body at 1200 K with added Gaussian noise

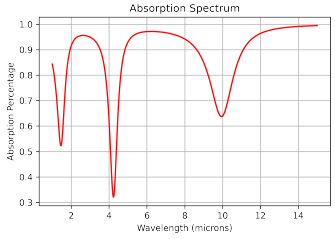

((b)) Sample transmission percentages across $1-15\mu m$ for a very simple atmosphere

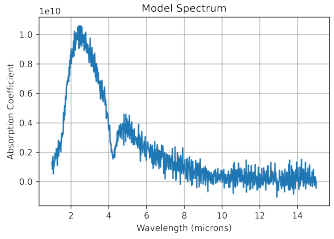

((c)) Combination of the model black body with absorption features

Figure 1.1 Figure 1.1(a) shows a basic light curve like what is emitted from the interior of a brown dwarf. Some of the light is absorbed as it passes through the atmosphere, which is represented by the transmission percentages in Figure 1.1(b). The resulting spectra picked up by the spectra would look something like that in Figure 1.1(c).

The resulting spectra are captured using a telescope and analyzed with a spectrograph to determine the amount of flux at different wavelengths. Spectra are the key to classifying brown

dwarfs into one of three different spectral types: L, T, and Y. The L dwarfs are the hottest of the three spectral types and have spectra marked by lines from alkali metals (such as cesium and rubidium) and bands from hydrides (compounds consisting of a metal and hydrogen) (Cushing 2013). Spectral types are an important part of classifying brown dwarfs but do not include precise information about the physical parameters and processes that characterize the atmosphere.

1.2 Forward Modeling

There are two principle methods for investigating brown dwarf atmospheres: retrieval and forward modeling. Retrieval modeling consists of developing a set of parameters which produce a model atmosphere and spectrum which matches the object being investigated. Forward modeling, a technique originally developed for exoplanet atmospheres, is a much faster technique that compares a bank of thousands of spectra produced using model atmospheres with varying parameters, such as temperature, metallicity, and the extent to which the atmosphere is stirred by cells of rising hot air (i.e. vertical mixing) to find the model that best fits the data (Marley et al. 2021). The goodness of fit is parameterized through some measure of error such as χ^2 (the squared difference between the values provided by the model and the observed spectra). The model spectra with the lowest error is the one generally used to make inferences about the brown dwarf.

Different models use different assumptions and calculation methods to create the atmosphere and resulting spectra. For example, all models will split up the atmosphere into layers with different properties, but individual models will vary in the way that they blend the layers together.

Model atmospheres also depend on accurate knowledge of the spectral characteristics of different molecules, meaning that advances in molecular spectroscopy necessitate a reevaluation of model atmospheres to include that new knowledge. For this reason, there are many different models to choose from when deciding how to characterize spectra.

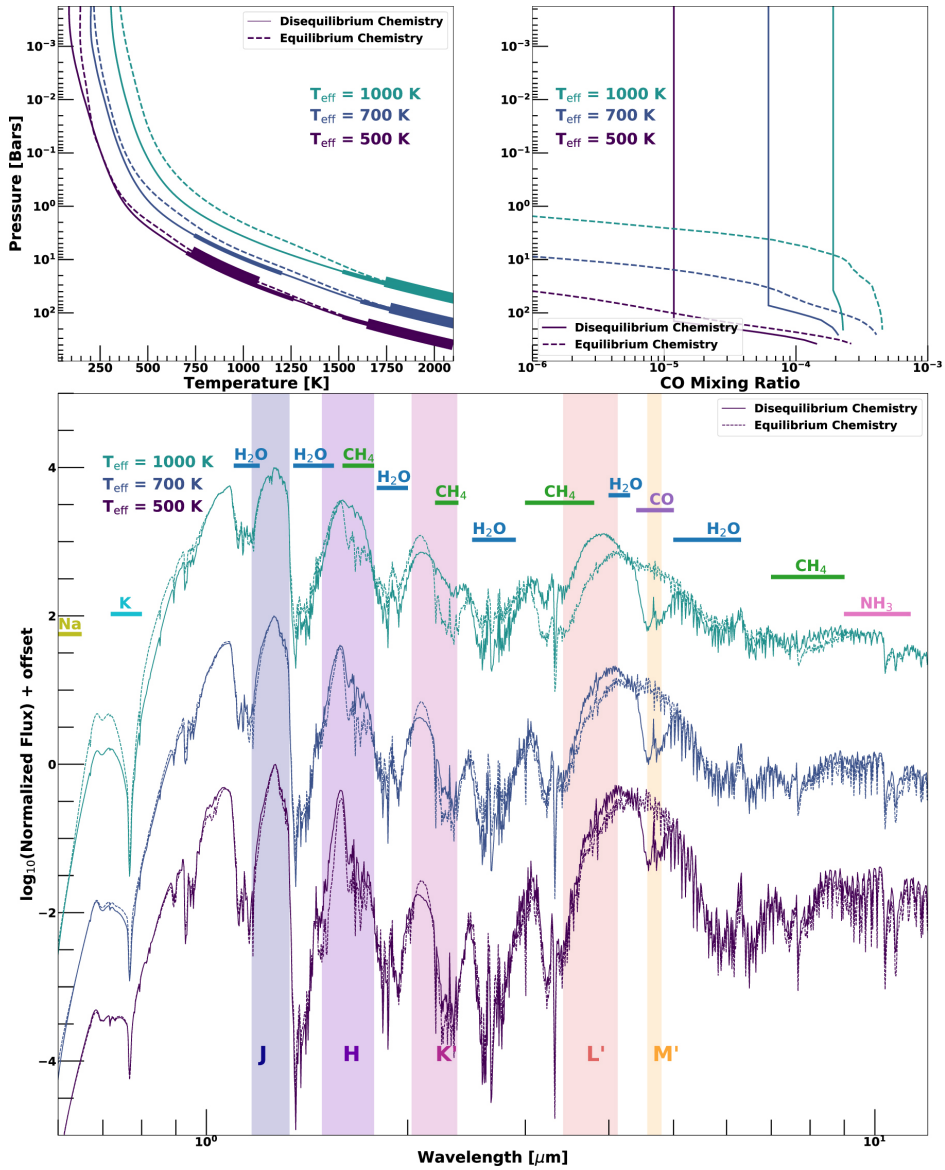

Figure 1.2 Figure 2 from Mukherjee et al. (2022) shows sample brown dwarf spectra annotated with the molecules commonly found in brown dwarf atmospheres and wavelength bands commonly used to describe spectra (J, H, K, and L'). Bluer colors correspond to cooler temperatures, which allow for the presence of different types of molecules. Cooler temperatures also allow for higher concentrations of certain types of molecules. These increasing concentrations can be seen in the larger and larger deviations from a black body curve under the black bars noting the absorption bands of molecules such as water (H_20) and methane (CH_4).

1.3 Model Overfitting and Underfitting

While all models aim to be as accurate as possible, the quality of our conclusions from forward modeling is limited to the quality of the models used in the analysis. For this reason, models that fit observed spectra well are critical to good analysis as they include the necessary compounds and physical processes to explain the resulting spectra.

Current models of brown dwarf atmospheres struggle to fit spectra for L-type brown dwarfs in two regions. Around $10\mu m$, models consistently overestimate the flux predicted in this range compared to what is observed. Suárez & Metchev (2022) explains this bad fit as a result of light scattering due to silicate clouds which have not been included in past model atmospheres. Morley et al. (2024) further explains that these silicate clouds are challenging to model using a single parameter.

The other region of poor fitting is from $3-5\mu m$, where models consistently underestimate the flux. This thesis demonstrates a tentative negative correlation between underfitting in the $3-5\mu m$ range and the $10\mu m$ feature considered by Suárez & Metchev (2022), suggesting a relationship between the presence of silicate clouds and the amount of flux emitted from $3-5\mu m$.

The rest of this thesis is organized as follows. In Chapter 2, I describe the sample of nine L dwarfs in the context of prior research, as well as the four instruments I obtained spectra from. I describe how I combined and analyzed the spectra as well as define a model underfitting index to guide my analysis. In Chapter 3, I report the results of forward modeling for the sample and the impact of combining spectra on predictions for physical parameters. I also analyze the relationship between model underfitting and the silicate deficit index defined by Suárez & Metchev (2022) and conclude a tentative negative correlation. Finally, in Chapter 4, I discuss the need for more high-quality data for early L dwarfs. I also suggest potential paths for future research.

Chapter 2

Methods

Prior to the launch of the James Webb Space Telescope (JWST), most telescopes used to analyze brown dwarf spectra only captured certain regions rather than the full wavelength range of relevant information. Now that JWST is online, telescope time is in high demand and the number of complete L-dwarf spectra is severely limited. In order to measure the spectra of objects in the wavelength ranges described above, it is necessary to combine spectra from different telescopes. For this study I have combined spectra from NASA's Infrared Telescope Facility (IRTF), the AKARI space telescope, and the Spitzer space telescope. I compare these combined spectra with two spectra obtained from JWST which cover the full wavelength range.

2.1 The Missions

Each of the telescopes used in this thesis, along with the relevant instruments, are discussed in this section.

2.1.1 IRTF Spex Telescopes

Located in Hawaii, IRTF is an observatory that splits its time between observations of solar system objects and other astronomical observing. The Spex instrument is a spectrograph which operates in the $0.8 - 5.5\mu m$ range. While operating in cross-dispersed mode, the instrument uses prisms to capture high-resolution spectra in the $0.8 - 2.4\mu m$ range (Rayner et al. 2003), which were retrieved for this thesis using the BD Simple database for brown dwarf photometry and spectroscopy (Cruz et al. 2023; Rodriguez & Cruz 2023). Spectra for two objects, 1507 and 2224, were obtained from Cushing et al. (2004).

Because this instrument operates from the ground, the spectra it captures are also filtered through Earth's atmosphere. Without correction, spectra from ground-based telescopes will have significantly less flux than those from space-based telescopes which are not contained within another layer of atmosphere. In order to avoid this problem, it is necessary to perform flux calibration, by which the comparison between the observed flux in the form of a magnitude and the expected magnitude is used to calculate a multiplicative factor to adjust the flux values upward.

As the IRTF data downloaded from the BD-Simple database was not marked as flux-calibrated or not, I compared the data downloaded from the database with with the AKARI data to see if the flux at the longest wavelengths of the IRTF data matched the flux at the shortest wavelengths of the AKARI data. The untouched data matched well with the AKARI data and so was used in this analysis.

2.1.2 AKARI Space Telescope

AKARI was a Japanese space telescope launched in 2006 and built to survey the sky from $1\mu m - 160\mu m$ using various instruments (Murakami et al. 2007). AKARI's IRC instrument provided spectroscopy from $1.8 - 26.5\mu m$. This study makes use of data from the NIR channel, which runs

from $1.8-5.5\mu m$. Because AKARI's IRC instrument covers the $3-5\mu m$ range, the data from this telescope are critical to evaluating the goodness of fit of current models.

Though AKARI was able to provide useful data for many different projects (as evidenced by the more than 750 times the paper describing the telescope has been cited as of the writing of this thesis), the telescope's observations of brown dwarfs in this channel suffer from high noise and objects being misaligned with the spectrograph slit. For this reason, the number of spectra of high enough quality for this thesis is limited.

2.1.3 Spitzer Space Telescope

The Spitzer Space Telescope was launched in 2003 into an orbit which trails behind the earth while providing data in the $3.6-160\mu m$ wavelength band (Werner et al. 2004). Data from this telescope revealed the model over- and underfitting that this thesis hopes to consider.

The Infrared Spectrograph (IRS) on the telescope provides high-resolution spectroscopy in the $5.3-38\mu m$ range. The short-low module on the instrument provided the data used in this thesis to construct composite spectra out to $15\mu m$. The IRS benefits from an autonomous system which ensures that objects are aligned with the spectrograph slit, thus limiting the problems encountered in the AKARI data (Houck et al. 2004).

The data used in this thesis was first published in Suárez & Metchev (2022).

2.1.4 James Webb Space Telescope

JWST was built to extend the work of the Hubble and Spitzer Space Telescopes using infrared observations (Gardner et al. 2006). The telescope includes two infrared spectrometers: the Near-Infrared Spectrograph (NIRSpec) and the Mid-Infrared Instrument (MIRI). The former instrument provides high-resolution spectra from $0.7-5.2\mu m$, while the latter runs from $5-28.5\mu$ (Jakobsen et al. (2022); Wells et al. (2015)). Combined spectra from the two instruments were presented in

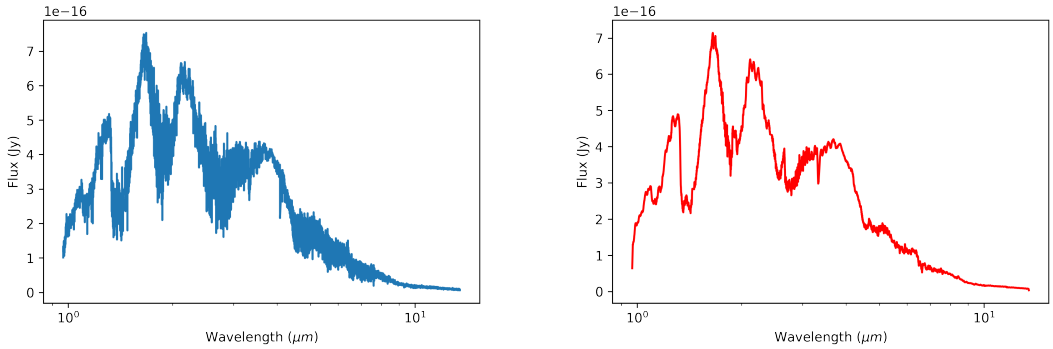

Figure 2.1 Side-by-side comparison of raw JWST data (left) with smoothed JWST data (right). Note how the absorption feature around $3.5\mu m$ is much clearer in the smoothed data than in the raw data. Also note how the possible absorption feature around $4\mu m$ vanishes in the smoothed data.

Miles et al. (2023) and are used here to analyze J1256 (See Table 2.1). An additional combined spectra was provided for this thesis by Lothringer (2023).

JWST's high resolution presents unique benefits and challenges. On the one hand, more information can be gleaned from high-resolution spectra than low-resolution. On the other, models have to be calculated at higher-resolutions to effectively make use of the data. In addition, effective interpretation of the data often requires that the data be smoothed so that spectral features can more easily be identified. Smoothing is achieved by calculating and recording a moving average for a given number of points. The higher the number of points, the greater the smoothing. See Figure 2.1 for a side-by-side comparison and discussion of the utility of smoothed JWST data.

2.2 Combining Spectra

Some of the spectra needed to be converted into units of Janskys (a unit of energy defined with respect to frequency space) to provide a common measurement as well as prepare the spectra for forward modeling. The AKARI and Spitzer data had known units of miliJanskys and Janskys respectively. The IRTF data downloaded was not marked with units and so it was necessary to

experiment with different conversion functions to figure out what the units of the spectra were. Using the Matplotlib Python library, I checked the magnitude of the units of the spectra conversions through visual inspection and selected the conversion that most closely mirrored the magnitude values for the AKARI and Spitzer data. I concluded the IRTF data was in units of erg s^{-1} cm^{-2} A^{-1}.

Visual inspection of 0825 revealed a slight offset in the magnitude of the longest wavelength AKARI data with the shortest wavelength Spitzer data. I applied of an offset of $-.5mJy$ to the Sptizer data to ensure that it matched with the AKARI data. This offset did not impact the results of the fitting, which are discussed in Chapter 3. After matching the ends of the spectra, I then used the NumPy python library to combine the data, remove missing data, and clip the spectra to $1-14.47\mu m$ in preparation for forward modeling.

2.3 The Sample

By compiling lists of the L-dwarf spectra from each of these instruments, I was able to check which objects had been observed with all three instruments and thus had spectra covering the full $1-15\mu m$ range. I was able to identify five objects in addition to the two objects observed by JWST (0624 & 1256) which are listed in Table 2.1. Two additional objects, 1507 and 2224, were identified from my research group's data archive.

Four of these objects; 0036, 0825, 1507, and 2224; were analyzed in Stephens et al. (2009) using models presented Saumon & Marley (2008). 0036 was identified in that study as a possible binary, but is treated here as a single brown dwarf to see if newer models can fit the object well without a companion. The global atmospheric parameters for these objects identified in Stephens et al. (2009) will be used as a point of comparison for the parameters I identify and will be discussed in Section 3.1.

Object	Short Name	Spectral Type
2MASS J00361617+1821104	0036	L3.5
2MASS J05395200-0059019	0539	L5
2MASS J06244595-4521548	0624	L6.5
2MASS J08251968+2115521	0825	L7.5
2MASS J08300825+4828482	0830	L9.5
2MASS J12560183-1257276	1256	L7
2MASSW J1507476-162738	1507	L5
2MASS J15232263+3014562	1523	L8
2MASSW J2224438-015852	2224	L4.5

Table 2.1 Sample of 9 L dwarfs with spectra from $1 - 15\mu m$

2.4 Model Families

I use two model families in the thesis: the Sonora family and the PHOENIX models. These are one-dimensional models which characterize atmospheres assuming that temperature and pressure only varies with altitude, leaving aside effects that are not spherically symmetrical and would thus require three dimensions to represent. The Sonora family of models was produced by the same team of researchers, while the PHOENIX models were developed independently. The two families are described in Sections 2.4.1 and 2.4.2.

There are two reasons for using multiple model families. First, using multiple model families allows me to check the parameters from one set of model results with the other model results and see how they compare. The second reason is that the two sets of models include different physical processes in their model atmospheres. This allows me to make conclusions about the physical processes that are most relevant for the spectra of one object.

Model Family	Clouds	Vertical Mixing/ Disequilibrium Chemistry
Sonora Bobcat		
Sonora Cholla		X
Sonora Diamondback	X	
PHOENIX	X	X

Table 2.2 Summary of physical processes considered in each model family

2.4.1 Sonora

The Sonora family of models are named for the region of desert in the United States of the same name. Each of the model subsets (Bobcat, Cholla, Diamondback, and soon to be published Elf-Owl) tackle a different combination of physical processes in their calculations.

The Sonora Bobcat models couple evolutionary models of brown dwarfs with atmospheric structure, thus providing better constrained physical properties than models which only consider atmospheric characteristics. The Bobcat models assume that there are no clouds on the brown dwarf, and that the rate of chemical reactions in the atmosphere is much faster than present transport mechanisms. This assumption is called chemical equilibrium. These models also assume radiative-convective equilibrium, in which the layers of the atmosphere where radiation is the most efficient means of energy transport do not move with respect to the layers where convection is the most efficient (Marley et al. 2021). The lack of clouds makes this family of models useful for early type dwarfs such as J0036.

The Cholla models are an iteration on a similar framework to the Bobcat models but with disequilibrium chemistry. With disequilibrium chemistry, the speed of chemical reactions is slower than other vertical transport mechanisms, allowing compounds to be dispersed throughout the atmosphere by convective mixing. Disequilibrium chemistry is a critical factor to consider when

analyzing exoplanet atmospheres, and the Cholla models were developed with that goal in mind (Karalidi et al. 2021).

Karalidi et al. (2021) notes that the Cholla models lack accurate alkali opacity data below $1.1\mu m$ and may not accurately represent the opacities relevant to the J-band. However, Because my research question most directly concerns the $3.5 - 11.5\mu$ range, these concerns do not disqualify the Cholla models from consideration.

The Diamondback models add clouds to the Bobcat models while maintaining conditions of chemical and radiative equilibrium. In addition, the Diamondback models implement updated lists of the spectral lines of the compounds present in brown dwarf atmospheres (Morley et al. 2024). The clouds are parameterized using the parameter f_{sed}, where larger clouds correspond to a lower f_{sed} value and smaller clouds correspond to a higher f_{sed} value.

The clouds in the Diamondback models do include silicate species, but Morley et al. (2024) warns that these silicates are unable to fit the silicate absorption feature from $9 - 10\mu m$. This inability is due to the use of a single parameter to classify clouds, which results in conditions that cannot replicate the feature. For this reason, I expect that any bad fitting resulting from the silicate feature will be still be present in the Diamondback models despite the presence of silicate clouds.

2.4.2 Phoenix

The code behind the PHOENIX models was initially presented in Hauschildt et al. (1992) to study the atmospheres of novae explosions. In subsequent years, the code was streamlined and applied to other, more stable stellar environments (Hauschildt et al. (1997); Hauschildt et al. (1999)). The code iterates through the layers of the atmosphere and adjusts the parameters describing the layer little by little until the full atmosphere reflects the desired global parameters (such as temperature and gravity) while also being self-consistent.

Due to the power of the code and its accompanying database of molecular spectral characteristics, PHOENIX was used in Brock et al. (2021) to study the properties of brown dwarf binary systems across the L/T transition. Across these spectral types, metals cool and condense into clouds, which impact the resulting spectra. Clouds are parameterized using the size of the cloud particles, where smaller cloud particles correspond to larger clouds and larger cloud particles correspond to smaller clouds (Brock et al. 2021). The PHOENIX models also include a vertical mixing parameter which describes the extent to which convective cells stir the atmosphere.

Though my sample covers earlier types than those considered in Brock et al. (2021), the PHOENIX model's inclusion of both clouds and vertical mixing provides a different set of assumptions to compare the results of forward modeling with the Sonora family of models.

2.5 Forward Modeling Procedure

To select the best fit model for each of the objects, I used the binary-fit Python program written by Savanah Turner (Turner 2024). Because the measured flux of an object is dependent on the distance between it and the observer, this program scales each model so that the flux values are of the same magnitude as the data. This scaling allows the models to be used independent of distance. In addition, binary-fit interpolates the models so that they have the same resolution as the data. This important step prevents extra detail being inferred where there is no data to support it.

Using the scaled and interpolated models, binary-fit calculates χ^2 values and then sorts the models from best-fitting to least-fitting using χ^2. The program reports detailed results for the top 200 models and records the name, χ^2 value, and scaling factor for the other models the object was compared against.

2.6 Defining Spectral Indices

The final piece required for this analysis is a numerical measure for how severely the models over or underfit the data. I adopt the silicate index described in Suárez & Metchev (2022) as a numerical parameterization for model overfitting. Figure 2.2 shows how the authors defined the index as the average flux of an interpolated linear function divided by the average flux of the data. A high silicate index corresponds to high overfitting and a large absorption feature.

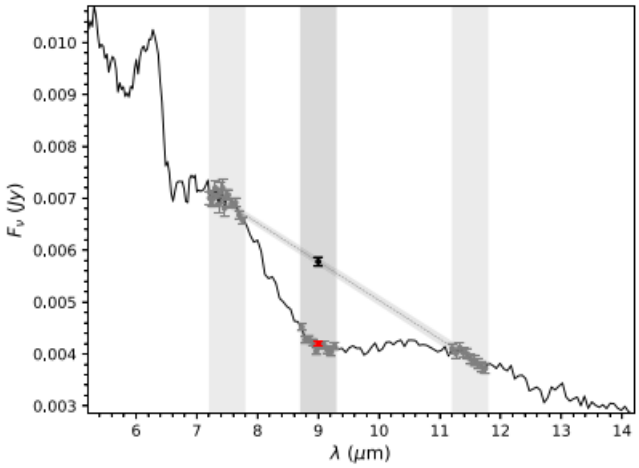

Figure 2.2 Figure 7 of Suárez & Metchev (2022) showing the definition of the silicate deficit index. A linear interpolation is calculated between the averages of the two regions marked by the outer grey bars. The average of the interpolated function is calculated for the inner gray bar (the black point) and divided by the average of the observed data (red point) to calculate the index.

Using a similar method, I define an underfitting index in $3.5 - 4.25\mu m$ range. These boundaries were selected using visual inspection to identify the wavelengths where underfitting tends to begin or end. To calculate the index, I integrate the data flux in this region and divide it by the integrated flux of the model in the same region to calculate an index describing the magnitude of underfitting (See Equation 2.2). The larger the index, the more the model underfits the actual data.

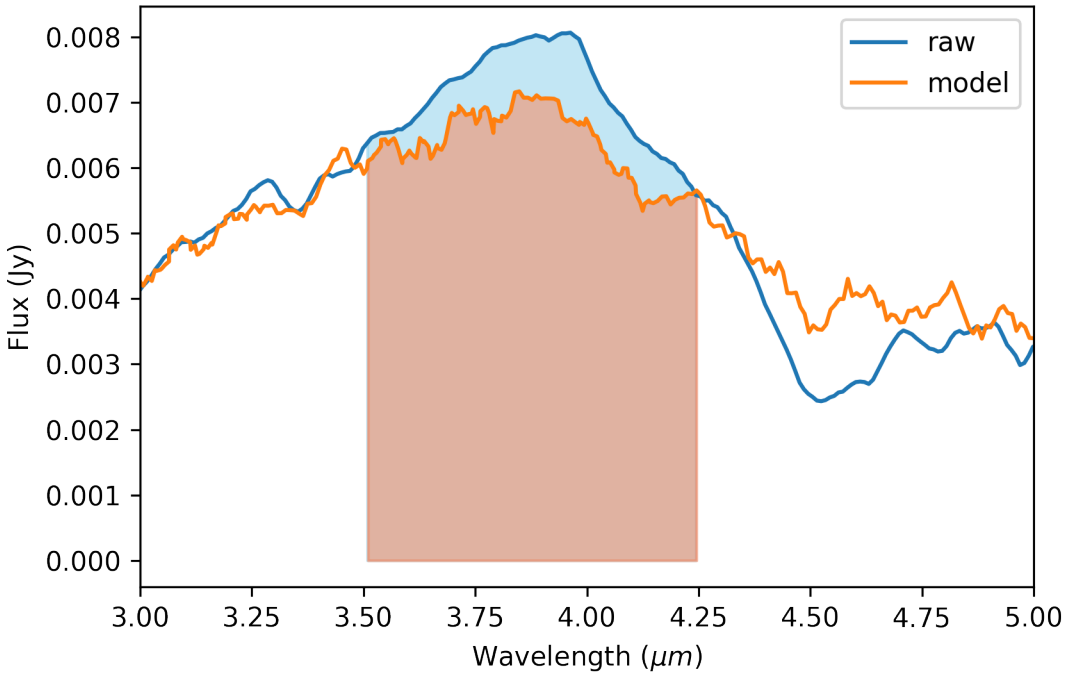

Figure 2.3 Graphical definition of the model underfit index. The flux for both the model and the observed data is integrated from $3.5\mu m - 4.25\mu m$. This integration is shown by the blue column in the background and the coral column in the foreground. The underfit index is defined as the integrated flux from the data over the integrated model flux.

The flux is integrated rather than averaged in this region because a black body curve in this region is not well approximated using linear functions. In addition, a numerical integral across this region is easier than trying to fit a function such as a parabola through the same reason and then taking the average of the parabola. The significance of a parameter defined using an integral is identical to the one defined by Suárez & Metchev (2022). To see why, consider the mathematical form of the silicate index in Equation 2.1.

$$\frac{\frac{1}{\lambda_2-\lambda_1}\int_{\lambda_1}^{\lambda_2} F_{\lambda,data}}{\frac{1}{\lambda_2-\lambda_1}\int_{\lambda_1}^{\lambda_2} F_{\lambda,model}} = n \tag{2.1}$$

Simple algebra reduces this equation to Equation 2.2.

$$\frac{\int_{\lambda_1}^{\lambda_2} F_{\lambda,data}}{\int_{\lambda_1}^{\lambda_2} F_{\lambda,model}} = n \tag{2.2}$$

Equation 2.2 is also the mathematical form of the underfit index. The difference is that $F_{\lambda,model}$ in the silicate index is linear while $F_{\lambda,model}$ in the underfit index is the model spectra.

Chapter 3

Results & Discussion

Results of forward modeling for each of the nine objects, along with values for all four indices are recorded in Tables 3.1 and 3.2. The temperature, clouds, mixing, and χ^2 values recorded in the table are those taken from the model with the lowest χ^2 value for the full combined spectra. The magnitude of the mixing parameter is proportional to the strength of vertical mixing.

Each object is described individually in the following section.

Obj	SpT	Silicate Index	Silicate Error	Underfit Index	Underfit Error
0036	3.5	1.2279	0.0122	1.0253	0.2×10^{-4}
0539	5	0.9622	0.0165	1.1122	0.6×10^{-5}
0624	6.5	1.3276	0.0005	1.0286	3.26×10^{-4}
0825	7.5	1.0607	0.0195	1.1053	1.3×10^{-5}
0830	9.5	0.5616	0.0704	1.1053	0.5×10^{-5}
1256	7	1.0529	0.0077	1.1740	1.712×10^{-3}
1507	5	1.1268	0.0089	1.0719	0.4×10^{-5}
1523	8	0.8389	0.0199	1.2154	0.4×10^{-5}
2224	4.5	1.4178	0.0200	1.0450	0.4×10^{-5}

Table 3.1 Index calculations for the full sample.

Obj	Temp (K)	Grav (log g)	Clouds (μm)	Mixing	Metallicity	C/O	χ^2	Notes
0036	2000	4.5	0.25	8	0	1	0.00604	
0539	1900	4.5	0.25	8	-0.5	1	0.00046	
0624	1800	5	0.25	8	0	1	27010.	1
0825	1700	5.5	0.25	8	0	1	0.00052	
0830	1450	5.2	0.25	4	0	1	0.00015	
1256	1300	5.5	0.5	4	0.5	1	0.00057	
1507	1900	4.5	0.25	8	-0.5	1	0.01849	
1523	1700	5.5	0.5	8	0	1	0.00004	2
2224	1800	5.5	0.25	8	0	1	0.00671	3

Table 3.2 Global parameter calculations for the full sample. Notes: 1) Though this χ^2 value is much higher than the other fits, this is because the units of the spectra are different from the other objects. The result is that the magnitude of the flux values from 0624 is 10^4 times that of the other objects, which results in a much higher χ^2 value. 2) Possible binary. 3) Atrocious fit with the models.

3.1 Discussion of Individual Objects

Due to the smallness of the sample and the variety of phenomena to address, this section considers each object, its model fit, and the interpretation of the data in its own section.

3.1.1 0036

Though 0036 was classified as a suspected binary in Stephens et al. (2009), a single component model does a reasonable job at fitting the object's spectrum. The best fit for the complete data was a high-temperature PHOENIX model with standard metallicity and C/O ratio. This suggests that the presence of clouds and vertical mixing are important components of the object's atmosphere.

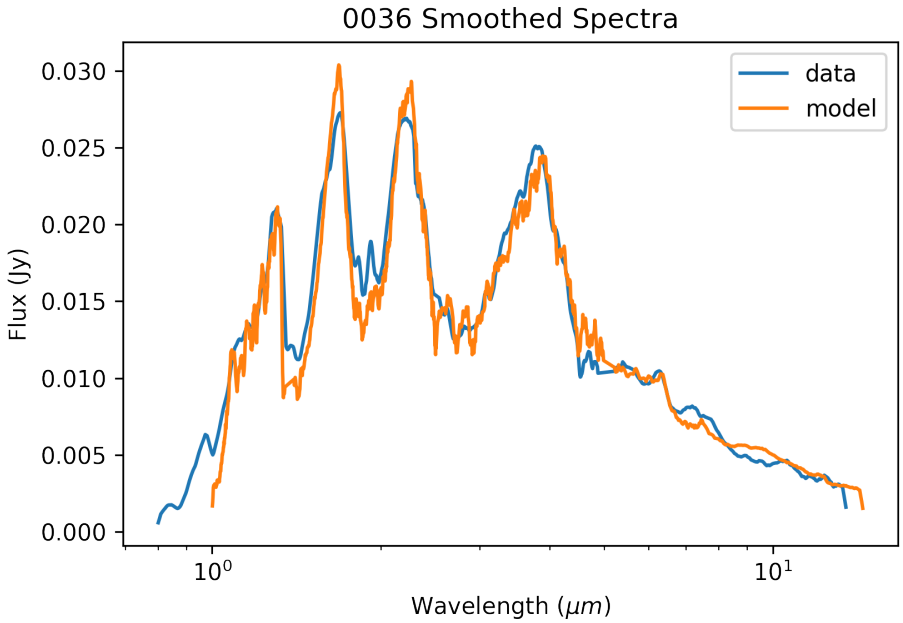

Figure 3.1 0036 combined spectra and best model fit smoothed across 7 adjacent cells.

The temperature calculated here is slightly higher than that recorded in Stephens et al. (2009), but the gravity value is consistent. Clouds and vertical mixing are parameterized differently between this thesis and Stephens et al. (2009), so direct comparison of the parameters is not possible. However, f_{sed} is proportional to grain size and so the f_{sed} value given in Stephens et al. (2009) (1) is consistent with my results.

The silicate feature at $10\mu m$ is clear in this spectrum and coincides with a lack of severe model underfitting from $3.5-4.25\mu m$. My calculated silicate index is within the error bars presented in Suárez & Metchev (2022) for this object. The model overfitting on the red side of the L' band can be interpreted as suppression of flux due to the presence of carbon monoxide.

The model overfits somewhat in the H and K bands as well as underfits between the two of them and between the J and H band. The overfitting may indicate more vertical mixing than that predicted by the model, as vertical mixing causes a drop in flux in these bands (see Figure 1.2). The underfit may be due to the presence of water, which absorbs light in these wavelength regions.

3.1.2 0539

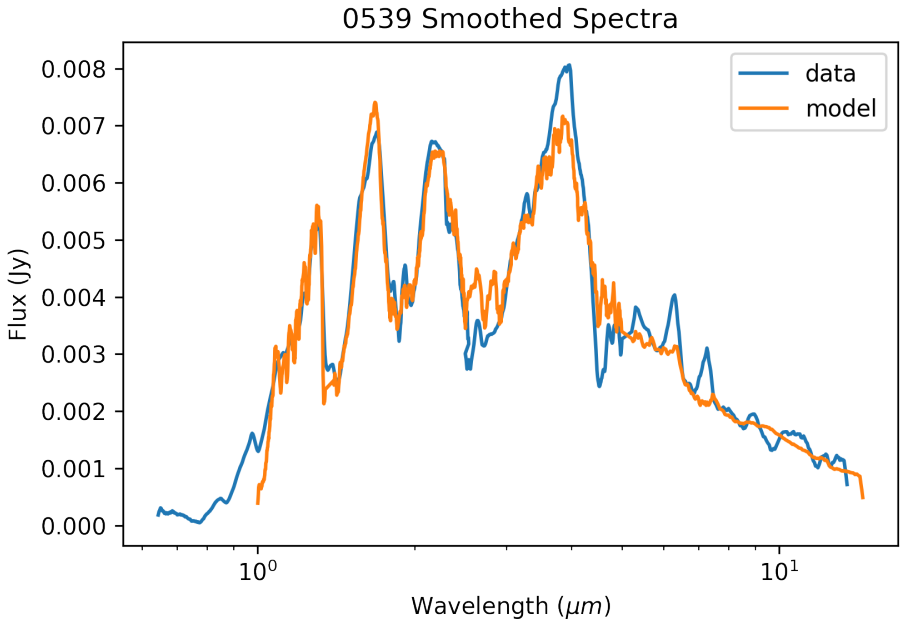

Figure 3.2 0539 combined spectra and best model fit smoothed across 7 adjacent cells.

0539's spectra was best fit using a high-temperature, low-metallicity PHOENIX model. As with 0036, this suggests that the combination of clouds and vertical mixing is best at describing this object.

The temperature calculated here is slightly higher than that presented in Gonzales et al. (2022), which preformed retrieval modeling on this object. The values for gravity calculated here are also much lower and the CO ratio is higher. The discrepancy between the temperature and CO ratio is a result of coarseness of the model parameter grid: as the differences between possible temperature and CO ratio values are large enough that the values in Gonzales et al. (2022) would fall between those in the grid.

The silicate index calculated here is within the error bars of that presented in Suárez & Metchev (2022). The feature is not as noticeable, but still recognizable in the Spitzer data.

The model overfits the regions on either side of the L' band, which can be interpreted as evidence for slightly higher absorption by CH_4 on the blue side of the band and CO on the red side of the band. The spikes in the data from $5-7\mu m$ may be artifacts from noise in the Spitzer data.

3.1.3 0624

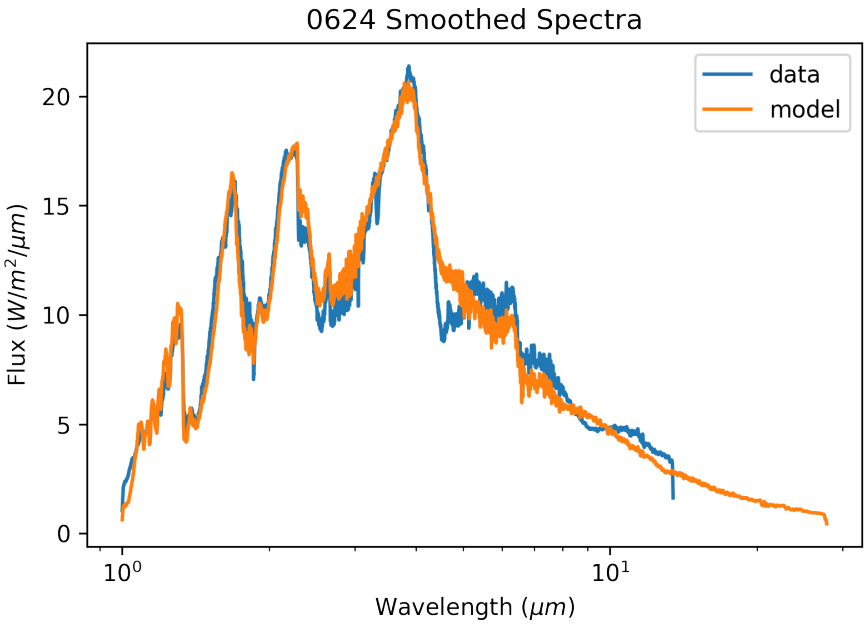

Figure 3.3 0624 combined spectra and best model fit smoothed across 35 adjacent cells.

This JWST spectra from 0624 was best fit using a PHOENIX model which fits very well through the J, H, K, and L' bands. Roberts (2024) fit this object using the Sonora family of models and calculated the temperature of the object to be 1600 Kelvin, which is slightly lower than the temperature calculated here. However, the Sonora models used in Roberts (2024) struggled to fit the $3.5-4.25\mu m$ feature where they did not here, indicating the importance of both clouds and vertical mixing to fitting this feature.

We do see the model overfitting from CH_4 and CO discussed previously, though it is more noticeable for CO than it is for CH_4. There is some model underfitting beginning at $5\mu m$ which appears as though all of the values are offset by a static amount.

The silicate value presented here is higher than that recorded for this object in Suárez & Metchev (2022). The difference is not surprising considering the extreme differences in resolution between JWST and Spitzer.

3.1.4 0825

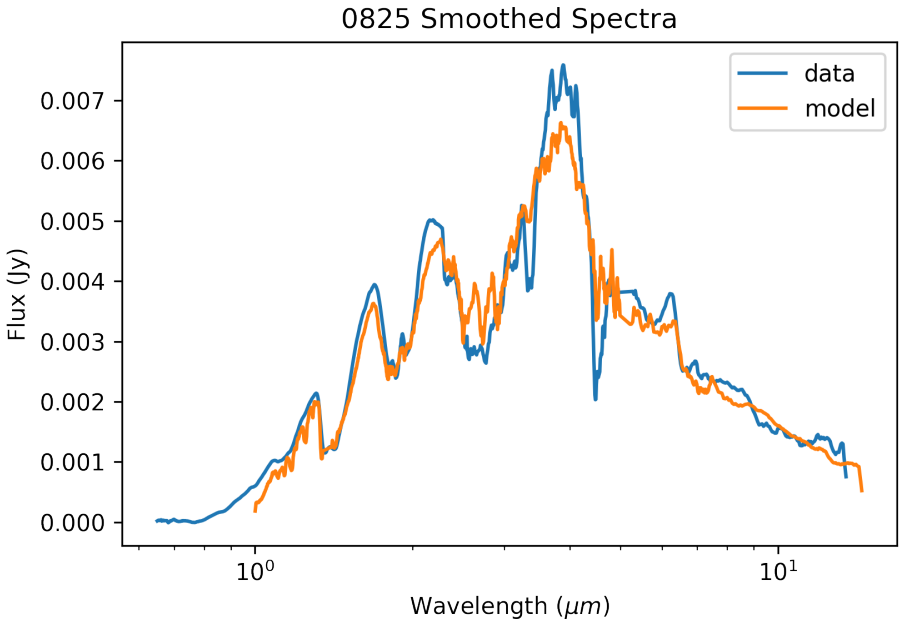

Figure 3.4 0825 combined spectra and best model fit smoothed across 7 adjacent cells.

0825 was best fit using a PHOENIX model with a temperature significantly higher than that presented in Stephens et al. (2009). The gravity value is consistent while the cloud parameter presented here corresponds to a slightly lower f_{sed} value than that in Stephens et al. (2009). The clarification in Section 3.1.1 applies here in interpreting the relationship between f_{sed} and PHOENIX's cloud parameter.

The silicate feature in 0825 is not as distinct as some of the other objects, but the index is consistent with that in Suárez & Metchev (2022). This is accompanied by significant model underfitting in the L' band and slight underfitting in the H and K bands. The underfitting in the K band may indicate less vertical mixing than that predicted by the model, as equilibrium chemistry is associated with higher fluxes in the K band (see Figure 1.1). CH_4 and CO absorption on either side of the L' band is shown through model overfitting in these regions.

3.1.5 0830

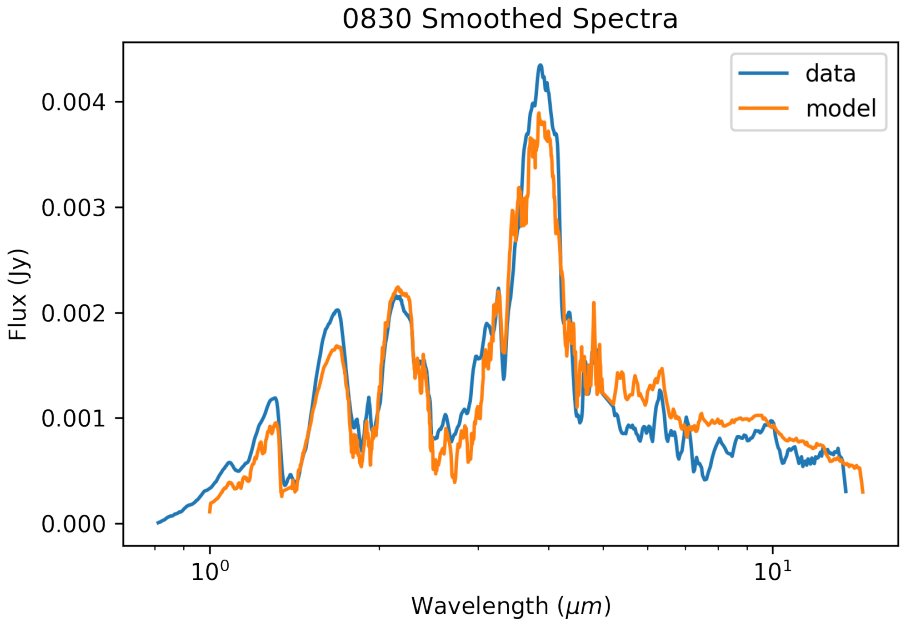

Figure 3.5 0830 combined spectra and best model fit smoothed across 7 adjacent cells.

0830 was best fit using a PHOENIX model. I was unable to find any other examples of modeling this object in the literature and so do not have any parameters to compare directly against. However, 0830 has the latest spectral type of the sample and, as expected, has the lowest predicted temperature.

The calculated silicate index is consistent with that presented in Suárez & Metchev (2022). The Spitzer data in this region is extremely noisy, which is reflected in the wide error bars in Suárez &

Metchev (2022). For this reason, combined with the great difference between the silicate indices of the other objects, this object's contribution to an overall relationship between silicate index and model underfit index should be cautious if not discounted entirely.

In addition to modest underfitting in the L' band, there is some underfitting in the J and H bands and between the K and L' bands. The latter underfitting may be due to lower absorption from CH_4 than predicted by the model.

3.1.6 1256

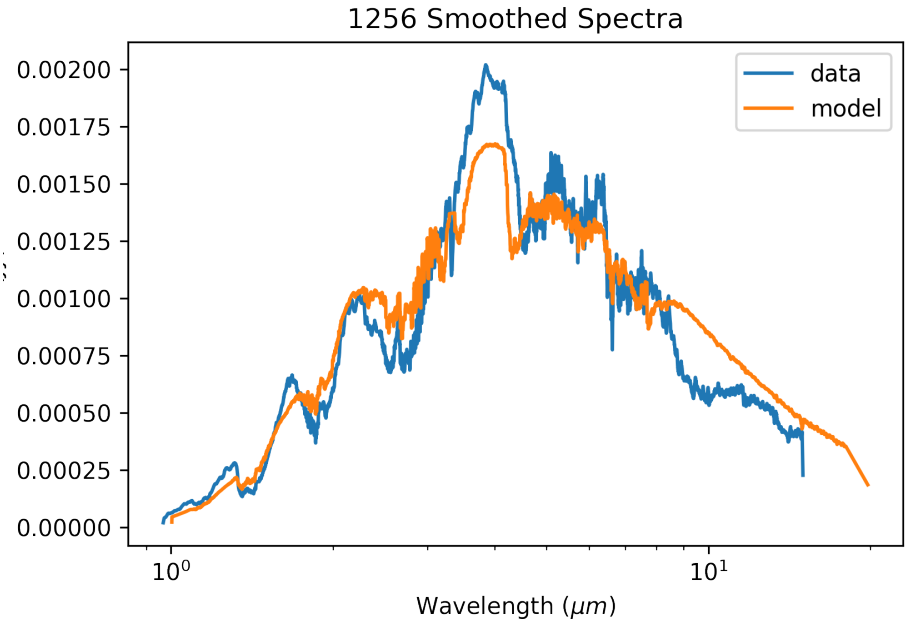

Figure 3.6 1256 combined spectra and best model fit smoothed across 35 adjacent cells.

1256's spectra was analyzed in detail in Miles et al. (2023). I will not reproduce the details here, but it is worth noting that the gravity value calculated here using a Sonora Diamondback model is the same as that presented in Miles et al. (2023) while the temperature is slightly higher. The fit from a Diamondback model is noteworthy because it is one of the only best fits that is not a PHOENIX model.

This study is the first to calculate a silicate index for this object. Despite the apparent depth of the absorption feature, the index is not the highest of those included in the sample. This absorption feature is accompanied by strong model underfitting in the L' band, as well as more moderate model underfitting in the J and H bands.

3.1.7 1507

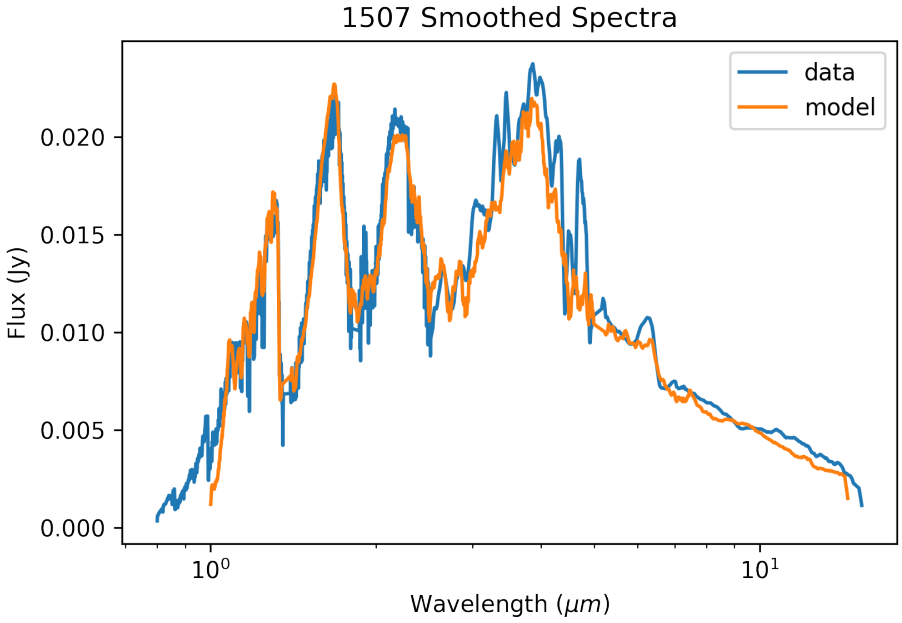

Figure 3.7 1507 combined spectra and best model fit smoothed across 7 adjacent cells.

1507 was best fit by a PHOENIX model with a temperature much higher than that presented in Stephens et al. (2009) (1900 K vs 1600 K). The resulting gravity value and cloud parameter are lower than those in Stephens et al. (2009), subject to the clarification explained in Section 3.1.1.

The silicate value calculated here is consistent with that presented in Suárez & Metchev (2022). The silicate feature is barely noticeable in the data and the model fitting is impressive in all other regions of the spectra. The model seems to capture all important features of the spectra extremely

well, suggesting that this object can almost entirely be described through a combination of clouds and vertical mixing.

3.1.8 1523

The initial fit for 1523 was very poor, prompting me to run a binary fit on the object. This consisted of testing different combinations of models and recording the combinations with the lowest error. The best fitting binary model is much better than the single-component fit. While this suggests that the object may be a binary, it is important to note that any system will be better fit by a more complicated system.

The binary fit for this object consists of two objects: a cloudless dwarf modeled by the Cholla models and a cloudy dwarf modeled by the Diamondback models. Complete parameters are shown in Table 3.3.

Component	Temperature	Gravity	Clouds	Mixing	Metallicity	C/O
Cloudless	1300	3.5	N/A	7	0	1
Cloudy	1400	5.5	1	N/A	0	1

Table 3.3 Global parameters for 1523's best fitting binary model. The Cloud field here is parameterized using f_{sed} rather than grain size.

Though it is possible that 1523 is actually two brown dwarfs, the fact that one model is cloudy and one is cloudless while having similar temperatures, metallicities, and C/O ratios suggests that 1523's atmosphere is not spherically symmetric. In this case, clouds would not be evenly distributed throughout the sky and so would allow light from deeper in the brown dwarf to escape. This would appear as a combination of a cloudy and a cloudless spectra as is the case here. The high vertical mixing parameter for the cloudless component is consistent with patchy clouds, as the regions not covered by clouds would provide a clear window into the gases stirred by convection.

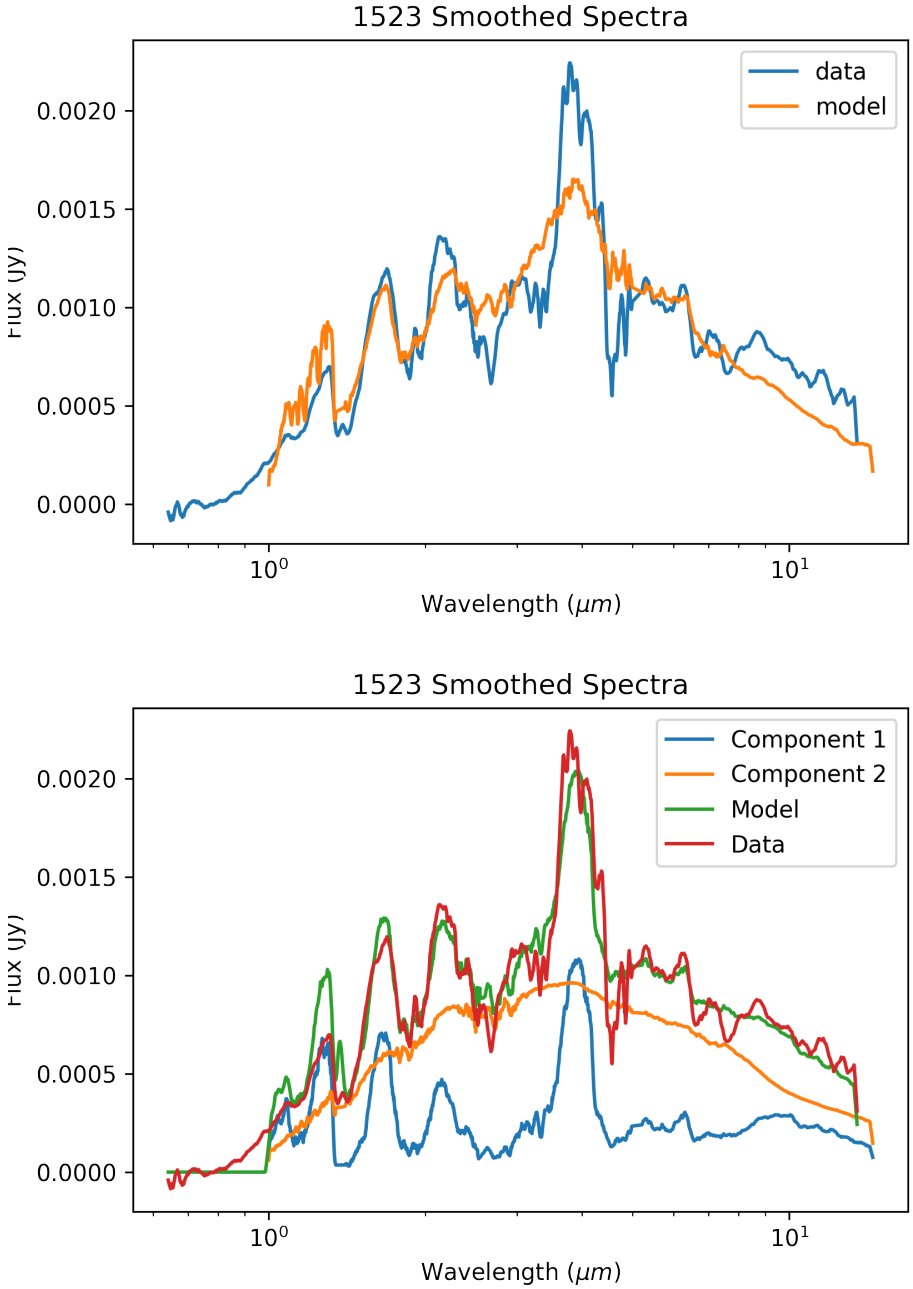

Figure 3.8 Side by side comparison of 1523's spectra with a single component fit and a binary fit. The binary fit does a much better job matching the data, though there is significant overfitting in the J and H bands.

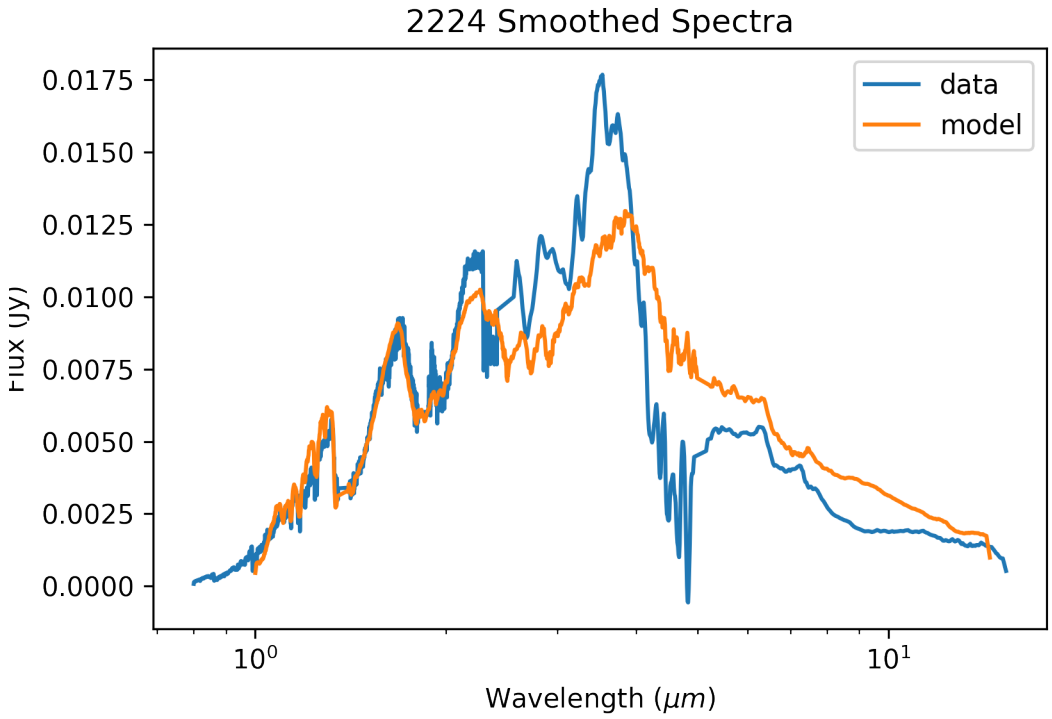

Figure 3.9 2224 combined spectra and best model fit smoothed across 7 adjacent cells.

If this object is a binary, it would require I omit its silicate index in a consideration of overall trends. It would not be clear which object was contributing to the deficit and to what degree. On the other hand, a non-spherically symmetric brown dwarf can be included in my analysis without issue. In any case, the calculated silicate index is consistent with that presented in Suárez & Metchev (2022).

3.1.9 2224

2224's PHOENIX best fit does not adequately fit the data to allow for extremely detailed analysis. When compared to the model fitting in Stephens et al. (2009), the temperature and gravity values calculated here are higher, while the cloud parameters are similar subject to the discussion in Section 3.1.1.

The silicate absorption feature is clear here, but the calculated index is lower than that recorded in Suárez & Metchev (2022). This may be due to a difference in treatment for the Spitzer data in Suárez & Metchev (2022) and that in my group's data repository.

3.2 A Negative Correlation Between the Slicate Index and the Underfit Index

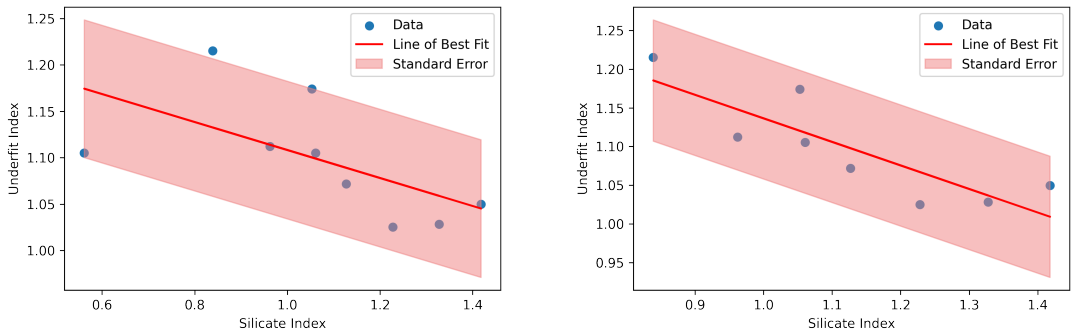

Figure 3.10 Single linear regression of the underfit index and the silicate index for the sample. The figure on the left shows the complete sample. Linear regression yields a correlation coefficient of -0.61 and a p value of 0.08. The figure on the right shows the results of linear regression if 0830 is removed from the sample due to its lower silicate index value. The correlation coefficient in this case is -0.85 and the p value is 0.008. Error values are omitted because further research is needed to define these values.

Figure 3.10 shows the results of linear regression on the sample when 0830 is included and when it is not (following the discussion in Section 3.1.5. In both cases, the line of best fit is clearly negative, though this is not a guarantee that there is a negative correlation between these parameters in the broader population of L dwarfs.

If this trend is reflected in L dwarfs generally, it would mean that the more pronounced the absorption feature at $10\mu m$, the less pronounced the model underfitting, implying the presence of silicates is consistent with more light in the $3.5-4.25\mu m$ range being emitted from the brown

dwarf. While it is possible that silicates may be absorbing light in the L' band and thus bring the flux nearer to the expected value, it is not clear why the presence of silicate clouds should be necessary to match the flux in the L' band in the first place. It seems more likely that there is a different condition that is responsible for the relationship. Perhaps the conditions that allow for silicate absorption at $10\mu m$ are also responsible for the goodness of fit by the cloudy models with disequilibrium chemistry.

Due to the smallness of the sample, these results are not definitive and should be interpreted conservatively as the sample may not be reflective of larger trends. Nevertheless, they do call for further study and verification, as this relationship may be important to consider in the refinement of our models of clouds in brown dwarf atmospheres.

3.3 The Impact of Combining Spectra

Normally, forward modeling is done with spectra collected from one instrument rather than composite spectra from multiple instruments. JWST is an exception to this general trend, as spectra from MIRI and NIRSpec are easily combined together for analysis. Because this thesis uses spectra combined from instruments that were not designed to work together, it is important to consider how the combination of spectra impacts the modeling results.

Extending the wavelength range of the spectra tends to constrain the possible values for both temperature and gravity when compared to spectra obtained from a single instrument, as shown in Figure 3.11. This constraining of values is not so significant that it shortens the range of possible values; rather, it makes it possible to identify the most likely combinations of temperature and gravity. This can be seen by comparing the subfigures in Figure 3.11 with each other. For the Spitzer data in the midle left, there is a broad spectrum of possible temperatures and a smaller spectrum of possible gravities while in the combined data in the bottom right, the possible combinations of

Objects	Ground Only	Akari Only	Spitzer Only	Ground + Akari	Akari + Spitzer	Combined
0036	1900	2100	1900	1800	2000	2000
0539	1900	1800	2300	1900	1800	1900
0825	1700	2100	1200	1700	1600	1700
0830	1797	1600	900	1450	1800	1450
1507	1900	1700	1900	1900	1800	1900
1523	1500	1700	1100	1778	1300	1700
2224	1700	2400	1900	1800	2400	1800

Table 3.4 Temperature values from forward modeling on different combinations of instrument spectra. All values are from the best fit single component model and are in units of Kelvin. 1507 and 2224 are known to be flux calibrated while the flux calibration of the other objects is unknown.

the two parameters are much more discrete. Other objects exhibit the same broad pattern in 1507's Spitzer data in the AKARI data.

When comparing the results of the model fits across the different instruments, the most probable value for temperature and gravity fluctuates sometimes quite wildly depending on which spectra is used to fit (See Table 3.4).

At the onset of this project, I did not know if all the IRTF data was flux calibrated. The objects that I know are flux calibrated (1507 and 2224) have fairly similar temperatures for the best-fitting model for the ground spectra as the combined spectra. The differences between these two wavelength spans is mostly reflected in the data from the other objects, though 0830's temperature derived from IRTF data is significantly higher than its combined spectra. These results suggest that either the data has been flux calibrated or that flux calibration usually does not make a difference in the atmospheric parameters derived using forward modeling.

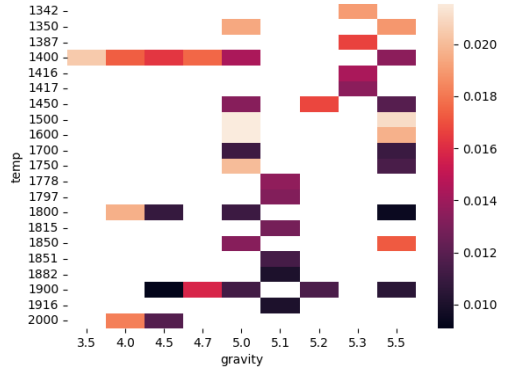

((a)) Errors for IRTF spectra

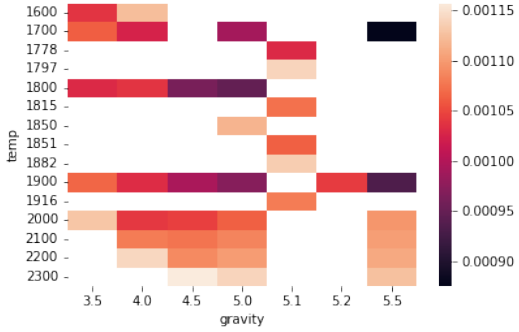

((b)) Errors for AKARI spectra

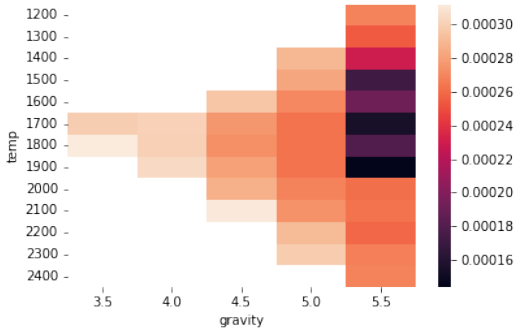

((c)) Errors for Spitzer spectra

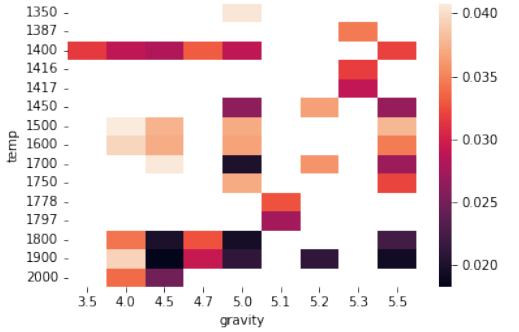

((d)) Errors for combined IRTF and AKARI spectra

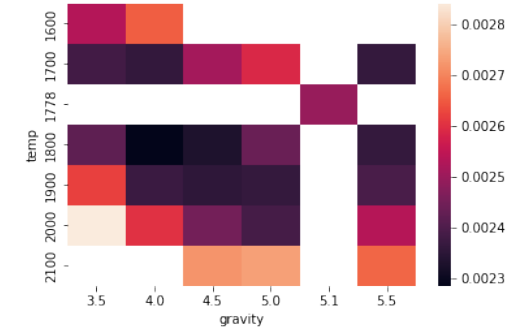

((e)) Errors for combined AKARI and Spitzer spectra

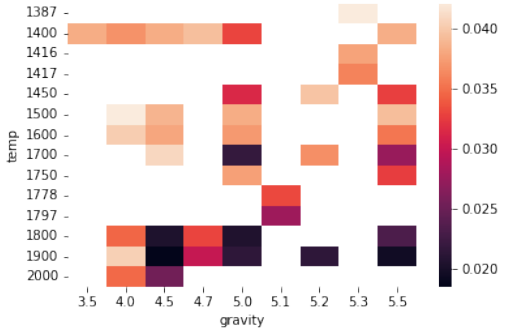

((f)) Errors for total combined spectra

Figure 3.11 Heat maps of possible temperatures and gravities for 1507 using different combinations of spectra. Darker colors are associated with lower errors in the fit and thus better quality.

Comparing the predicted temperature values from different instrument spectra shown in Table 3.4 shows that the combination of all three spectra consistently results in a temperature value that is at least reasonable, even if the specific temperature varies somewhat from those contained in the literature.

Chapter 4

Future Work

4.1 Quantifying Errors for Index Values

Error values are needed to robustly analyze these index values. The methods that I tried to quantify the error were moderately successful, and so further research is needed.

An important component of this error calculation would be determining errors for the model fits. Though the heat maps presented here help to show the error in global parameters like temperature, they do not provide insight into the error of the flux values for the model. My attempt to quantify the error consisted of taking the standard deviation of the flux values for the top 200 models fit to the data. This was a good beginning, but the error values for the silicate index were significantly higher than those reported in Suárez & Metchev (2022). Future research could focus on using other statistical methods to quantify the error in the model.

4.2 More Effects of Combining Spectra

Due the smallness of my sample, my conclusions about combining spectra are extremely limited. Not all of these objects would need to be L-dwarfs, as I suspect the effects of combining spectra

would be more impacted by the number and type of telescope spectrometers than by the spectral type. A large sample of brown dwarfs could be used to consider many more variables than I treated here, such as cloud grain size and vertical mixing.

Better information about the impact of combining spectra on the results of forward modeling would help researchers more effectively plan requests for telescope time, as it would clarify how archival spectra could be used in conjunction with new spectra.

4.3 Follow-up Observations and Calculations

Though the ensemble of global parameters presented in Section 3.1.8 are compelling, the gravity values for the two components are reversed of what we would expect if the spectra described a non-spherically symmetric system. We would expect a higher gravity value to go with the denser, cloud-free brown dwarf core and a lower gravity value to go with the less-dense, cloudy atmosphere.

The most direct way to determine whether or not this is a binary system would be to observe the system with a powerful enough telescope to resolve the individual objects. Barring this course of action, there are spectral indices which suggest binarity (Bravo et al. 2023). These indices could be used as indirect evidence for or against the binarity hypothesis for this object. A third method would be to use three-dimensional models to see if spherical asymmetries would improve a single-component fit.

The six other objects considered using combined spectra can be further investigated using retrieval modeling methods such as those that are available using the Planetary Intensity Code for Atmospheric Scattering Observations (PICASO, see Mukherjee et al. (2023)). Retrieval modeling is able to create more personalized models at the cost of speed, which would allow for direct testing of variations in model parameters with model fitting. Bartier (2024) will include retrieval models

for some of these objects, and these models could then be used to consider the relationship between silicate absorption and L' band underfitting.

4.4 The Need for More JWST Data

There are several other avenues for extending this thesis. The Sonora Elf-Owl models presented in the forthcoming Mukherjee (2024) have a larger ranger of metallicities and could be used to probe the influence of metallicity on the silicate and underfit indices. In addition, if models could be developed which use multiple cloud parameters to fit the $10\mu m$ silicate feature, these models could be used to test whether the conditions which create the feature still fit the L' band well.

Both of these suggestions would require more objects to analyze. Dropping the requirement for IRTF Spex data would be a reasonable way of expanding the sample, however doing so wouldn't add any new L dwarfs to this sample based on my current list of objects in the AKARI and Spitzer data. If any new objects were to be identified in the data, predictions for temperature measurements based on the combination of AKARI and Spitzer data might or might not be consistent with the temperature that would be predicted if the full spectrum were fit to forward models. In addition, the predicted gravity values could be underestimated with respect to the full spectrum in some cases.

The other way to add more objects to the sample would be to observe more objects across the $3-15\mu m$ range. The James Webb Space Telescope (JWST) has instruments which can capture the full length of brown dwarf spectra with much greater resolution that previous telescopes. The first of these spectra have been collected and are currently undergoing analysis (Lothringer (2023); Miles (2023)). While these first L dwarf spectra have yielded and will yet yield new insights into their atmospheric dynamics, many more are needed to be able to make statistically robust conclusions for the entire population. Recent JWST investigations have focused on Y and T brown dwarfs, as they are much dimmer than L dwarfs and so the number of telescopes with the ability to observe them is

limited. This thesis demonstrates the need for more L-dwarf spectral data, whether that be the full $1-15\mu m$ range or the $3-5\mu m$ range, and JWST is the most powerful option for collecting those spectra. Expanding the number of high-quality, wide spectra available for all brown dwarfs will enable researchers the ability to make exciting discoveries about the way that atmospheres work, allowing us to better understand what skies exist on other worlds.

Appendix A

Heat Graphs of Sampled Objects

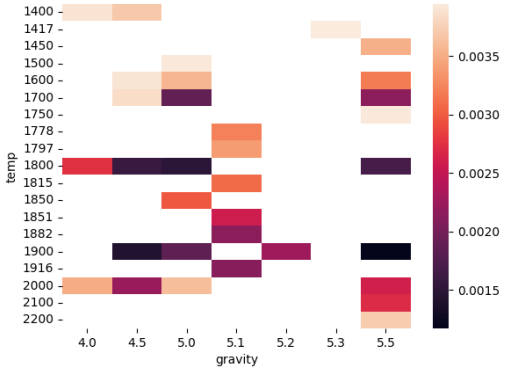

((**a**)) Errors for IRTF spectra

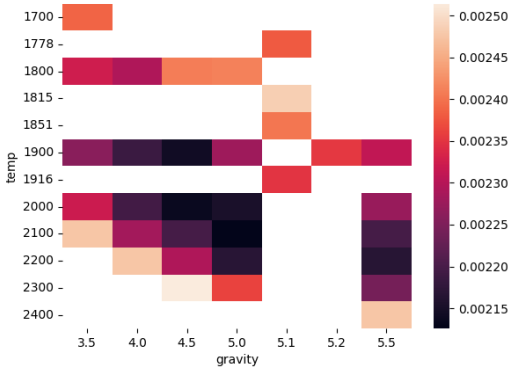

((**b**)) Errors for AKARI spectra

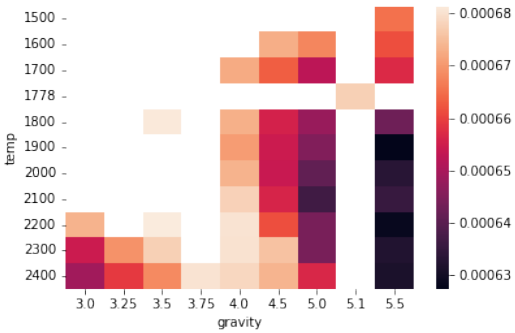

((**c**)) Errors for Spitzer spectra

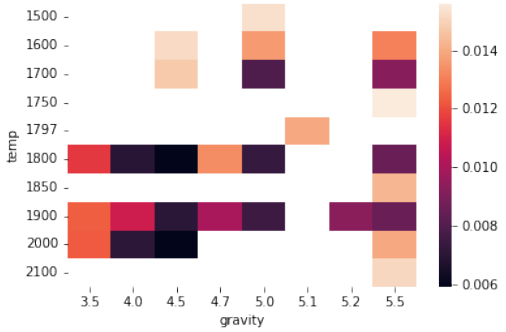

((**d**)) Errors for combined IRTF and AKARI spectra

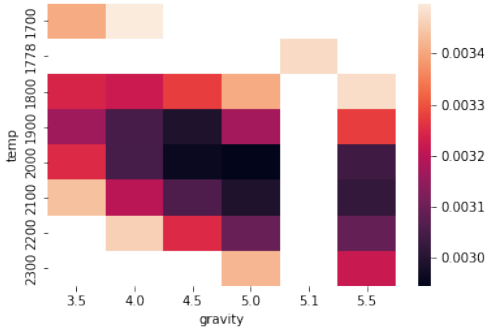

((**e**)) Errors for combined AKARI and Spitzer spectra

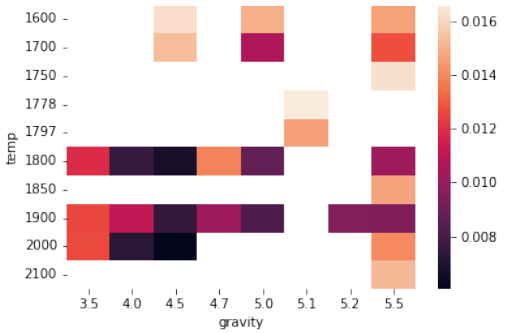

((**f**)) Errors for total combined spectra

Figure A.1 Heat maps of possible temperature and gravity values for 0036 using different combinations of spectra. Darker colors are associated with lower errors in the fit and thus better quality.

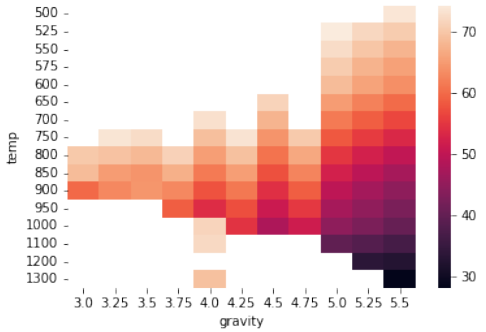

((**a**)) Errors for IRTF spectra

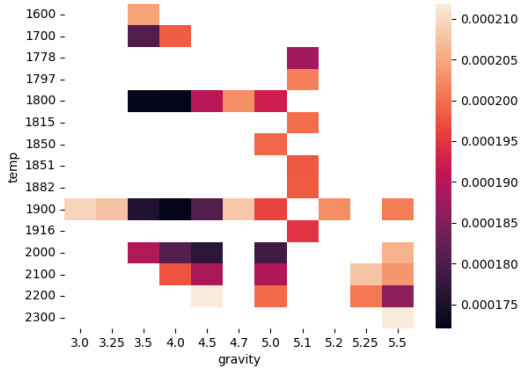

((**b**)) Errors for AKARI spectra

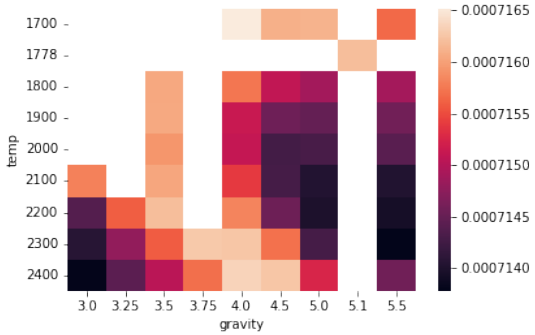

((**c**)) Errors for Spitzer spectra

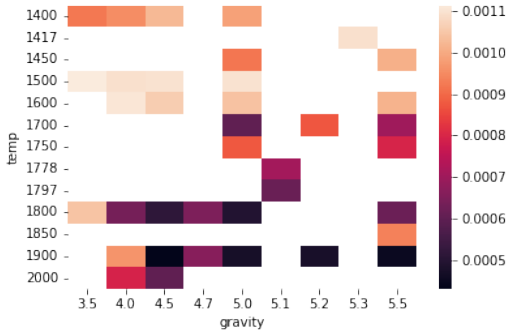

((**d**)) Errors for combined IRTF and AKARI spectra

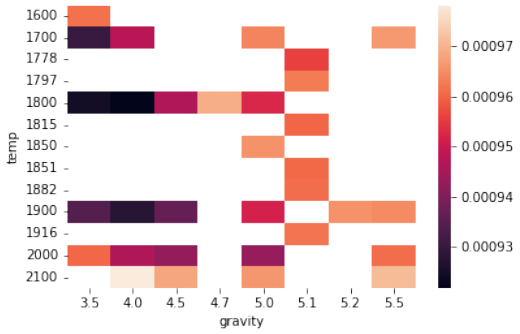

((**e**)) Errors for combined AKARI and Spitzer spectra

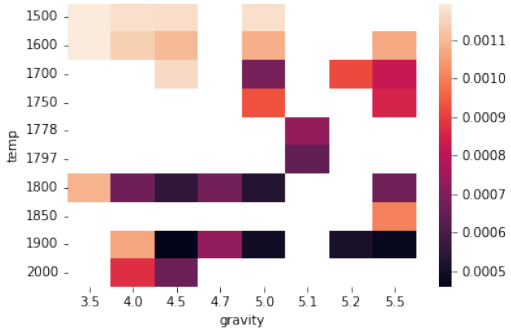

((**f**)) Errors for total combined spectra

Figure A.2 Heat maps of possible temperatures and gravities for 0539 using different combinations of spectra. Darker colors are associated with lower errors in the fit and thus better quality.

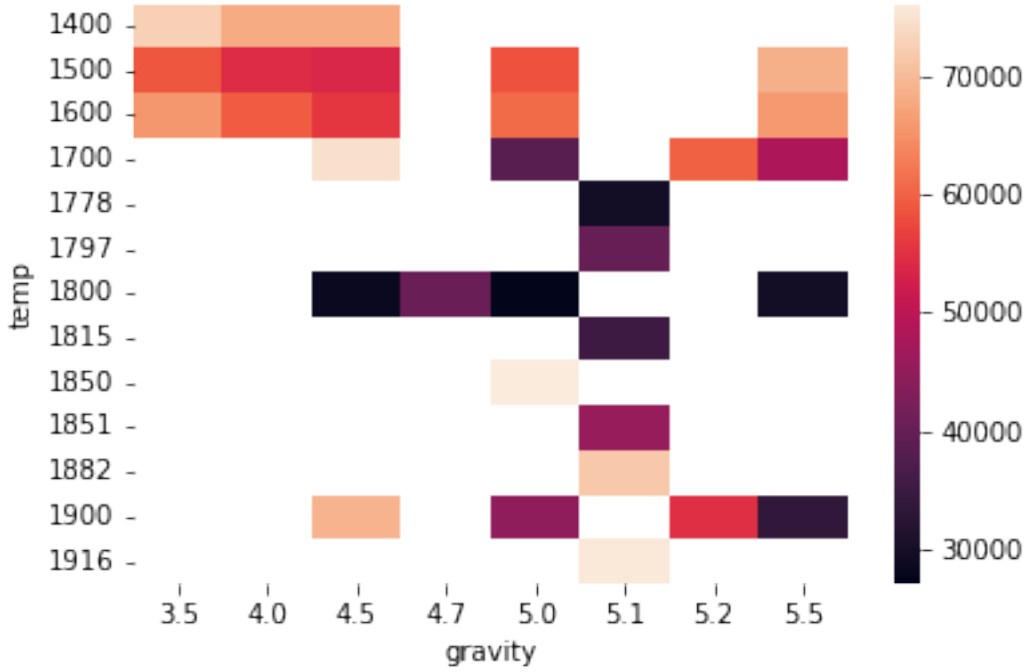

Figure A.3 Heat map of possible temperatures and gravities for 0624. Darker colors are associated with lower errors in the fit and thus better quality.

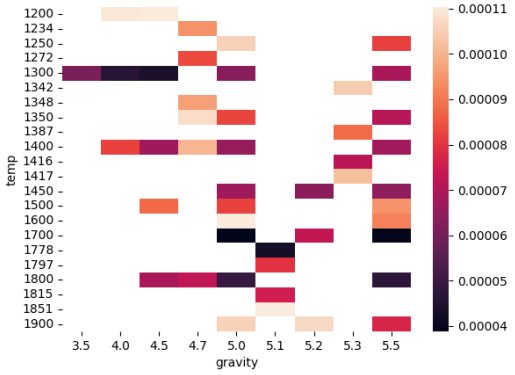

((a)) Errors for IRTF spectra

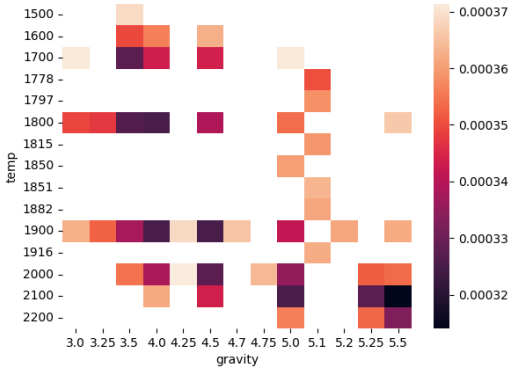

((b)) Errors for AKARI spectra

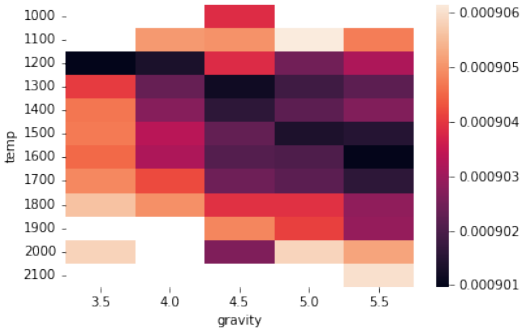

((c)) Errors for Spitzer spectra

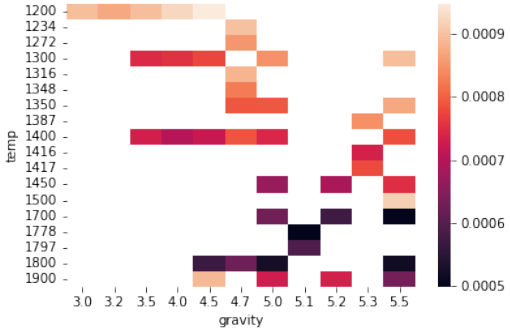

((d)) Errors for combined IRTF and AKARI spectra

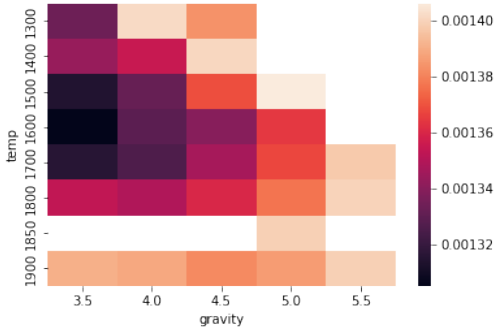

((e)) Errors for combined AKARI and Spitzer spectra

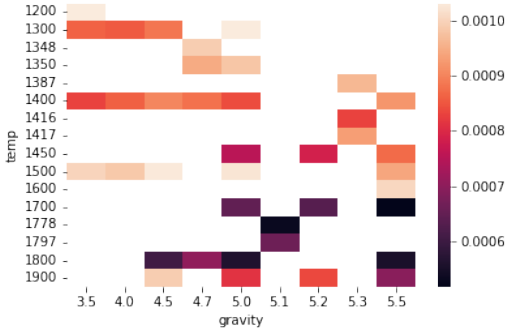

((f)) Errors for total combined spectra

Figure A.4 Heat maps of possible temperatures and gravities for 0825 using different combinations of spectra. Darker colors are associated with lower errors in the fit and thus better quality.

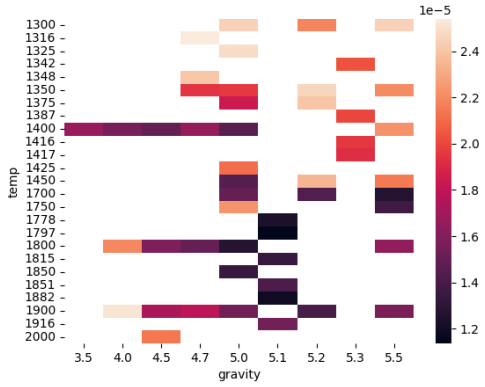

((a)) Errors for IRTF spectra

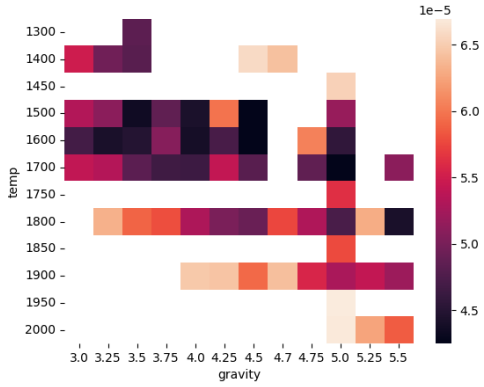

((b)) Errors for AKARI spectra

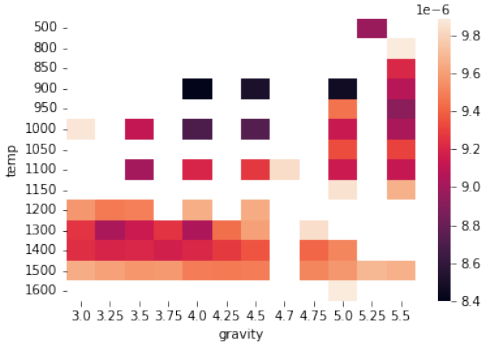

((c)) Errors for Spitzer spectra

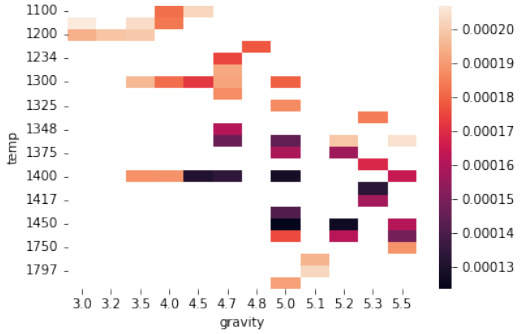

((d)) Errors for combined IRTF and AKARI spectra

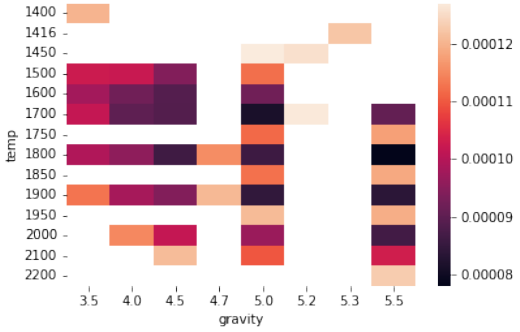

((e)) Errors for combined AKARI and Spitzer spectra

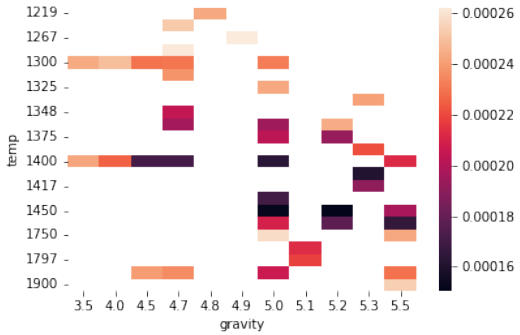

((f)) Errors for combined spectra

Figure A.5 Heat maps of possible temperatures and gravities for 0830 using different combinations of spectra. Darker colors are associated with lower errors in the fit and thus better quality.

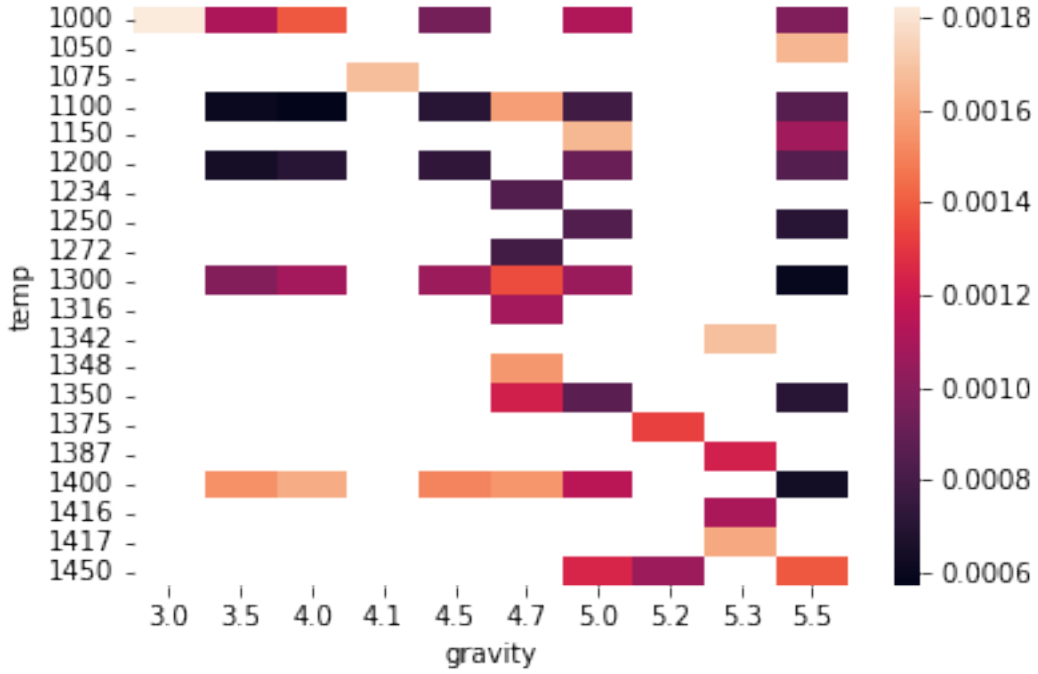

Figure A.6 Heat map of possible temperatures and gravities for 1256. Darker colors are associated with lower errors in the fit and thus better quality.

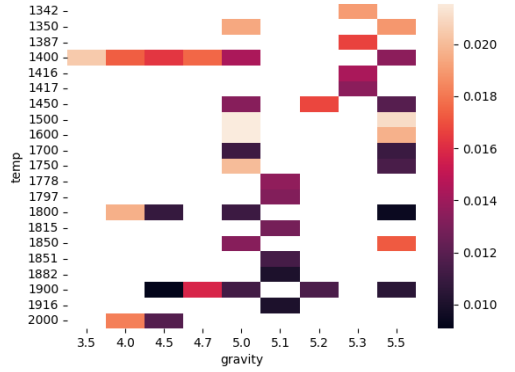

((**a**)) Errors for IRTF spectra

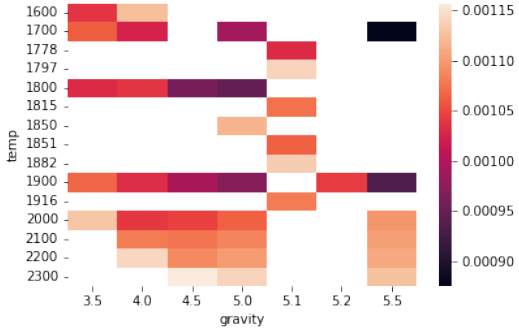

((**b**)) Errors for AKARI spectra

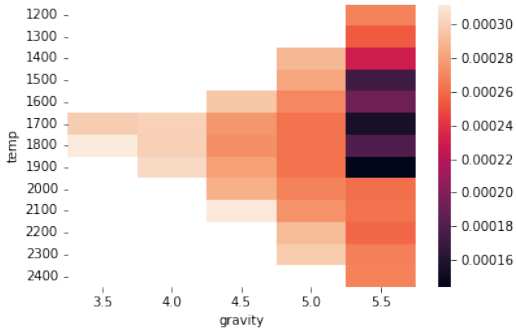

((**c**)) Errors for Spitzer spectra

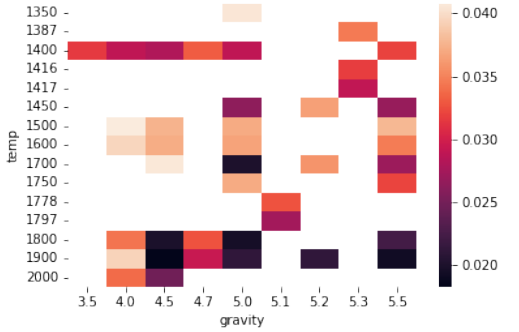

((**d**)) Errors for combined IRTF and AKARI spectra

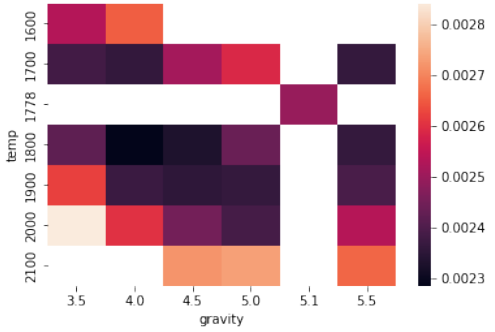

((**e**)) Errors for combined AKARI and Spitzer spectra

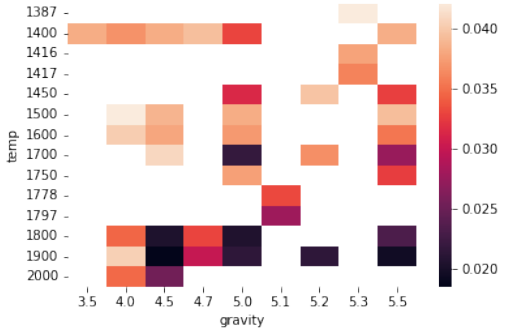

((**f**)) Errors for total combined spectra

Figure A.7 Heat maps of possible temperatures and gravities for 1507 using different combinations of spectra. Darker colors are associated with lower errors in the fit and thus better quality.

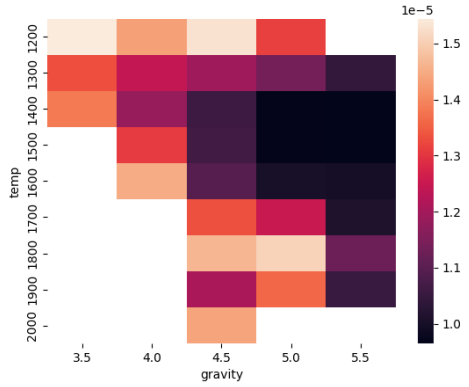

((a)) Errors for IRTF spectra

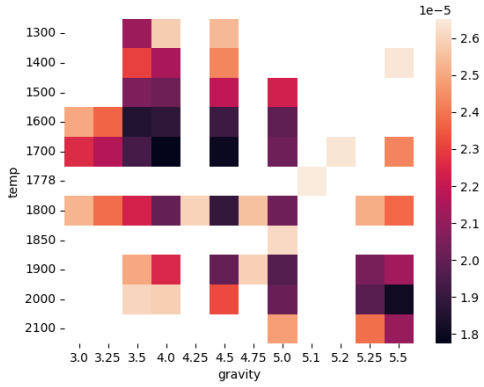

((b)) Errors for AKARI spectra

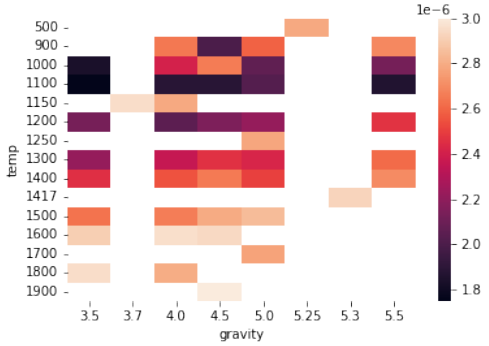

((c)) Errors for Spitzer spectra

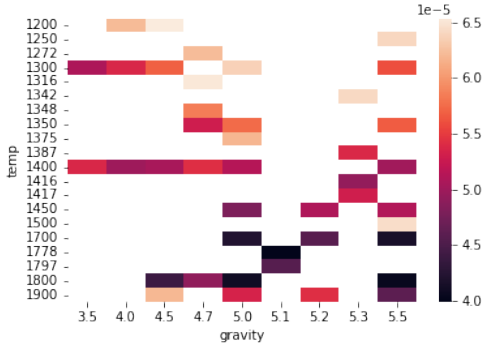

((d)) Errors for combined IRTF and AKARI spectra

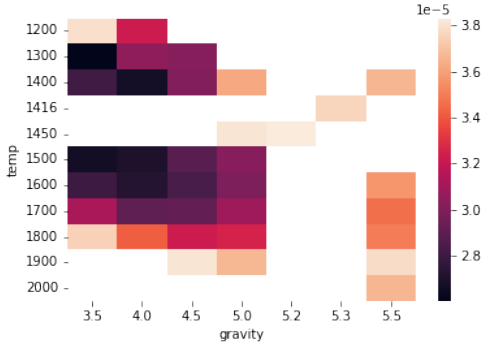

((e)) Errors for combined AKARI and Spitzer spectra

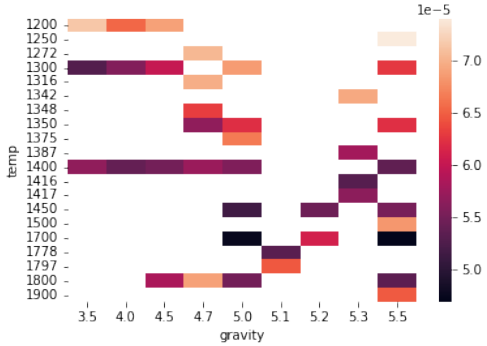

((f)) Errors for total combined spectra

Figure A.8 Heat maps of possible temperatures and gravities for 1523 using different combinations of spectra. Darker colors are associated with lower errors in the fit and thus better quality.

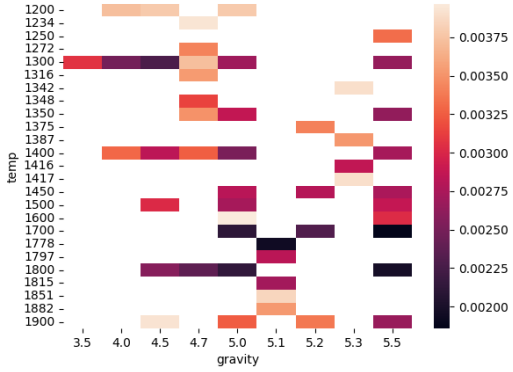

((a)) Errors for IRTF spectra

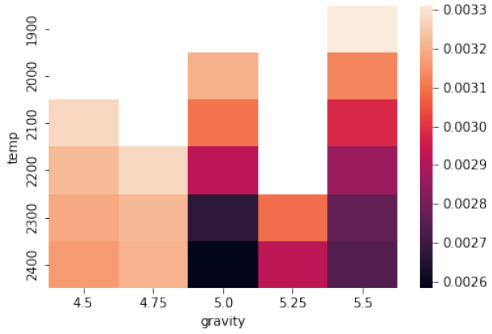

((b)) Errors for AKARI spectra

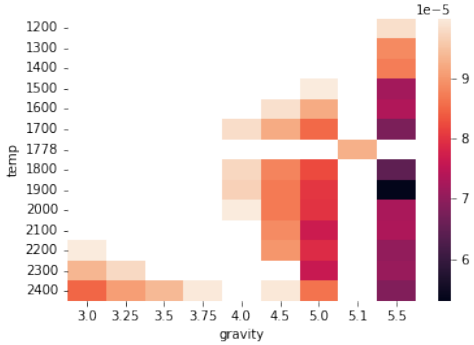

((c)) Errors for Spitzer spectra

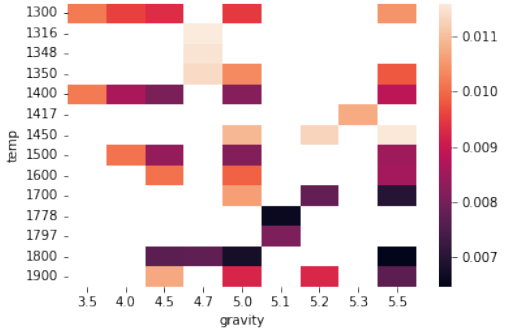

((d)) Errors for combined IRTF and AKARI spectra

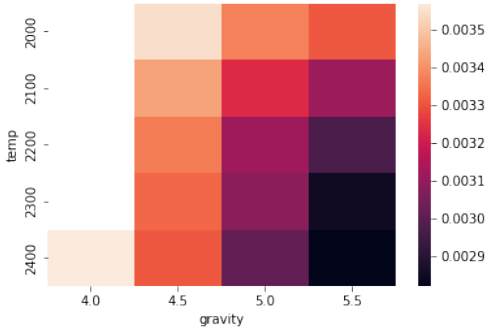

((e)) Errors for combined AKARI and Spitzer spectra

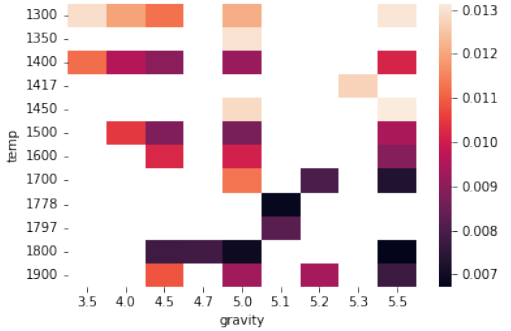

((f)) Errors for total combined spectra

Figure A.9 Heat maps of possible temperatures and gravities for 2224 using different combinations of spectra. Darker colors are associated with lower errors in the fit and thus better quality.

Bibliography

Bartier, C.-L. 2024, in prep.

Bravo, A., et al. 2023, AJ, 166, 226

Brock, L., Barman, T., Konopacky, Q. M., & Stone, J. M. 2021, The Astrophysical Journal, 914, 124

Cruz, K., Cooper, W., Rodriguez, D. R., Alejandro, S., Hort, E., Fontanive, C., & Whiteford, N. 2023, The SIMPLE Archive: A collaboratively-curated database and website of low mass stars, brown dwarfs, and exoplanets

Cushing, M. C. 2013, 50 years of brown dwarfs, 2014th edn., ed. V. Joergens, Astrophysics and Space Science Library (Basel, Switzerland: Springer International Publishing)

Cushing, M. C., Vacca, W. D., & Rayner, J. T. 2004, PASP, 116, 362

Dupuy, T. J., & Liu, M. C. 2017, ApJS, 231, 15

Gardner, J. P., et al. 2006, Space Sci. Rev., 123, 485

Gonzales, E. C., Burningham, B., Faherty, J. K., Lewis, N. K., Visscher, C., & Marley, M. 2022, ApJ, 938, 56

Hauschildt, P. H., Allard, F., & Baron, E. 1999, ApJ, 512, 377

Hauschildt, P. H., Baron, E., & Allard, F. 1997, ApJ, 483, 390

Hauschildt, P. H., Wehrse, R., Starrfield, S., & Shaviv, G. 1992, ApJ, 393, 307

Houck, J. R., et al. 2004, The Astrophysical Journal Supplement Series, 154, 18–24

Jakobsen, P., et al. 2022, A&A, 661, A80

Karalidi, T., Marley, M., Fortney, J. J., Morley, C., Saumon, D., Lupu, R., Visscher, C., & Freedman, R. 2021, The Astrophysical Journal, 923, 269

Kumar, S. S. 1962, AJ, 67, 579

Lothringer, J. 2023, Private communication

Marley, M. S., et al. 2021, The Astrophysical Journal, 920, 85

Miles. 2023, Private communication

Miles, B. E., et al. 2023, ApJ, 946, L6

Morley, C. V., et al. 2024, arXiv e-prints, arXiv:2402.00758

Mukherjee, S. 2024, submitted

Mukherjee, S., Batalha, N. E., Fortney, J. J., & Marley, M. S. 2023, The Astrophysical Journal, 942, 71

Mukherjee, S., Fortney, J. J., Batalha, N. E., Karalidi, T., Marley, M. S., Visscher, C., Miles, B. E., & Skemer, A. J. I. 2022, ApJ, 938, 107

Murakami, H., et al. 2007, PASJ, 59, S369

Oppenheimer, B. R., Kulkarni, S. R., Matthews, K., & Nakajima, T. 1995, Science, 270, 1478

Rayner, J. T., Toomey, D. W., Onaka, P. M., Denault, A. J., Stahlberger, W. E., Vacca, W. D., Cushing, M. C., & Wang, S. 2003, Publications of the Astronomical Society of the Pacific, 115, 362

Roberts, B. 2024, in American Astronomical Society Meeting #243

Rodriguez, D., & Cruz, K. 2023, The SIMPLE Archive

Saumon, D., & Marley, M. S. 2008, ApJ, 689, 1327

Stephens, D. C., et al. 2009, ApJ, 702, 154

Suárez, G., & Metchev, S. 2022, MNRAS, 513, 5701

Turner, S. 2024, in prep.

Wells, M., et al. 2015, PASP, 127, 646

Werner, M. W., et al. 2004, ApJS, 154, 1

Index